NASA-TM- 83558

NASA Technical Memorandum 83558

Three-Dimensional Viscous Design Methodology For Advanced Technology Aircraft Supersonic Inlet Systems

FOR REFERENCE

NOT TO BE TAKEN FROM THIS ROOM

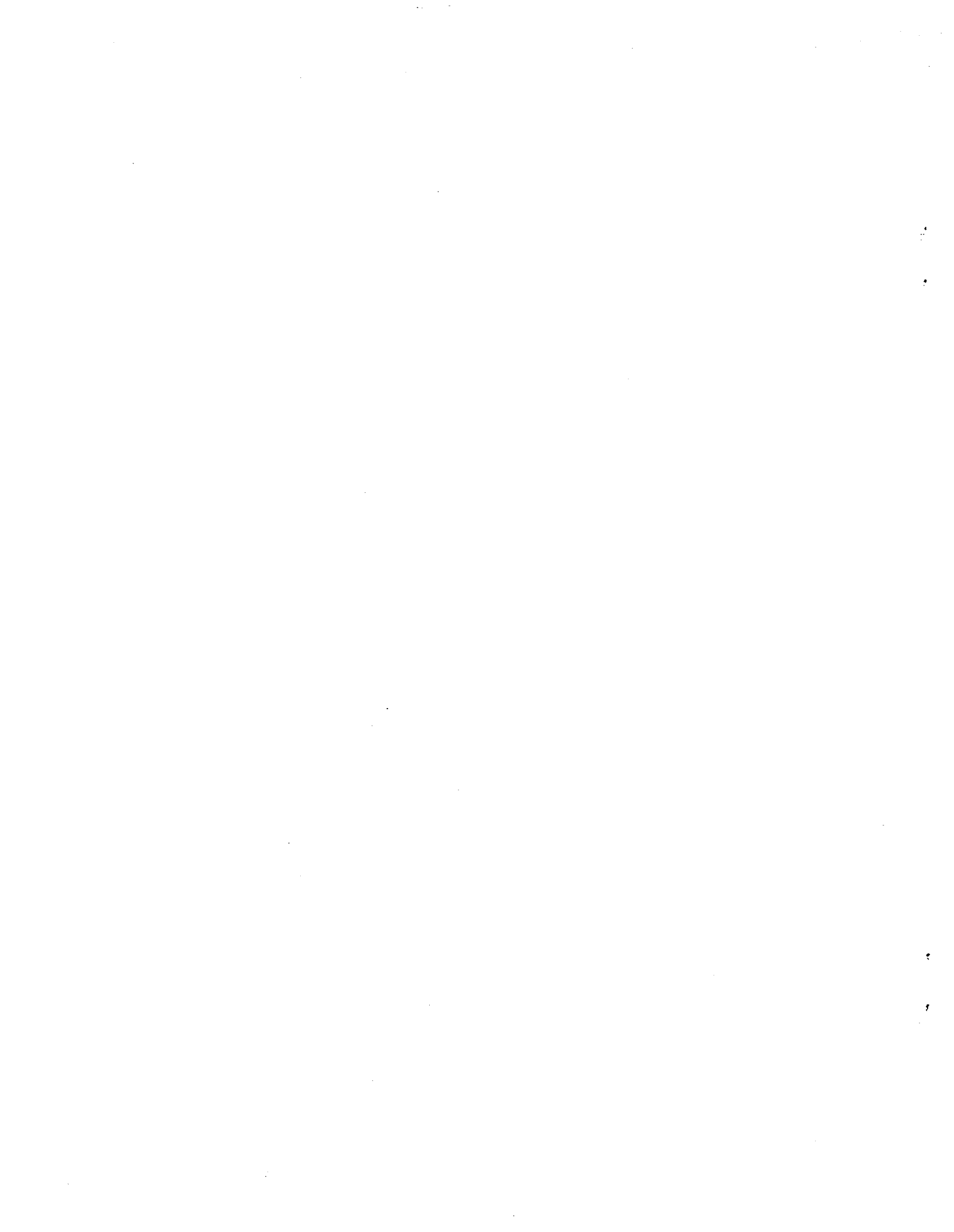Bernhard H. Anderson
Lewis Research Center
Cleveland, Ohio

NASA

UTTL: Three-dimensional viscous design methodology for advanced technology
    aircraft supersonic inlet systems
AUTH: A/ANDERSON, B. H.
CORP: National Aeronautics and Space Administration. Lewis Research Center,
    Cleveland, Ohio.   AVAIL.NTIS   SAP: HC A04/MF A01
    Presented at the 21st Aerospace Sci. Meeting, Reno, Nev., 9-12 Jan. 1984
MAJS: /*AIRCRAFT ENGINES/*INLET FLOW/*SUPERSONIC INLETS/*THREE DIMENSIONAL FLOW
    /*VISCOUS FLOW
MINS: / AERODYNAMICS/ COMPUTATIONAL FLUID DYNAMICS/ COMPUTER AIDED DESIGN/
    ENGINE DESIGN
ABA: Author
ABS: A broad program to develop advanced, reliable, and user oriented
    three-dimensional viscous design techniques for supersonic inlet systems,
    and encourage their transfer into the general user community is discussed.
    Features of the program include: (1) develop effective methods of
    computing three-dimensional flows within a zonal modeling methodology; (2)
    ensure reasonable agreement between said analysis and selective sets of
    benchmark validation data; (3) develop user orientation into said
    analysis; and (4) explore and develop advanced numerical methodology.

ENTER:

THREE-DIMENSIONAL VISCOUS DESIGN METHODOLOGY
FOR ADVANCED TECHNOLOGY AIRCRAFT SUPERSONIC INLET SYSTEMS

Bernhard H. Anderson
National Aeronautics and Space Administration
Lewis Research Center
Cleveland, Ohio 44135

SUMMARY

The present report discusses a broad program to develop advanced, re-
liable, and user oriented three-dimensional viscous design techniques for
supersonic inlet systems, and encourage their transfer into the general user
community. This program is fourfold in nature, namely (1) develop effective
methods of computing three-dimensional flows within a zonal modeling metho-
dology, (2) ensure reasonable agreement between said analysis and selective
sets of benchmark validation data, (3) develop "user" orientation into said
analysis, and (4) explore and develop advanced numerical methodology.

INTRODUCTION

Calculation of the extremely complex multidimensional viscous flow fields
found in supersonic inlet systems proposed for advanced technology aircraft
presents difficult but necessary challenges. Although one method of determin-
ing a suitable design system would focus upon an extensive testing program,
the costs of hardware fabrication and individual tests are such that an alter-
nate, more efficient design procedure is required. One method which is cur-
rently being pursued at NASA Lewis Research Center focuses upon the development
of a series of computer codes to predict the aerodynamics of supersonic inlet
systems in general geometries operating at realistic flow conditions. When
developed further, these analyses could be used to (1) examine basic flow
mechanisms governing the flow field under study, (2) give guidance to new and
more efficient component designs, (3) predict the system operation at various
flight conditions, and (4) reduce the experimental test matrix. All these
items would be of significant value to the design engineer.

The broad objective of the program at NASA Lewis Research Center is to
develop advanced, reliable, and user oriented computer design techniques for
advanced supersonic inlet systems and encourage their transfer into the general
user community.

(1) Develop effective methods of computing the three-dimensional viscous
flow fields within supersonic inlet systems using Spatial Marching and Navier
Stokes techniques within an overall zonal calculational methodology.

(2) Generate a significant benchmark experimental data base against which
said analyses may be verified; determine the range of applicability and accur-
acy of said analyses, and provide guidance for improving these analyses by
comparison with benchmark experimental data.

E-1936

N84-13190#

(3) Develop "user orientation" into these analyses which includes graphical output representation, case "running" protocol for flows of interest, and a formalized structure to use these three-dimensional codes.

(4) Explore the development of improved three-dimensional grid generation, numerical methodology, and computer technology utilization relative to supersonic inlet analyses.

ZONAL ANALYSIS METHODOLOGY

Generation of analyses for predicting the viscous flow in advanced supersonic inlet systems represents a difficult but important problem. The flow field in physically realistic situations is three-dimensional, viscous (and usually turbulent), and contains strong shock waves. One method of developing an analysis for these flow fields would focus upon the solution of the three-dimensional Navier Stokes equations. Although these equations could be used in principle for the entire flow field of interest, the number of grid points required to obtain adequate flow resolution is prohibitive and makes this approach impractical even for the next generation of computers.

A suitable alternative which has been pursued by the Aerodynamic Analysis Section at the NASA Lewis Research Center is the zonal embedding methodology. Under this philosophy the overall flow field is divided into distinct parts and each part analyzed via the appropriate set of equations. Interaction between sections may be considered as required. The use of zonal embedding methods is advantageous in several ways, namely (1) the region over which the complex equations are used is minimized, (2) the simpler sets of equations have faster algorithms which result in improved computational efficiency and (3) the computer storage requirements for the overall procedure are not as great. All of these advantages lead to more cost effective computer analyses.

An example of the zonal embedding methodology is illustrated in figure 1, which is developed for three-dimensional supersonic inlet systems. The flow in the supersonic portion of the inlet will be calculated using the three-dimensional PEPSIS general flow field solver. Downstream of the inlet throat in the subsonic portion of the inlet diffuser, the flow will be computed using the PEPSIG general flow solver. Interfacing these two regions is the inlet throat. Within this region, there is supersonic flow upstream of the normal shock wave and subsonic flow on the downstream side. In this region of the inlet, the flow field will be analyzed using the three-dimensional generalized MINT computer code. The computations in this region would be numerically interfaced with the upstream PEPSIS calculation and the PEPSIG downstream solution. A similar zonal methodology was developed for the analysis of forced mixer nozzles and nonaxisymmetric nozzle systems.

In general, the flow fields of interest can be analyzed via one or more of the following approaches: (1) supersonic three-dimensional viscous spatial marching solvers, (2) subsonic three-dimensional viscous spatial marching solvers, and (3) three-dimensional inviscid/viscous elliptic solvers. Generalized analyses for each of these approaches have been developed and validated against both laminar and turbulent benchmark experimental data. These Generalized Three-Dimensional Flow Solvers are called the PEPSI/MINT series of computer codes and are described in the appendix. The PEPSIS computer code

(refs. 1 to 5) was developed as a generalized three-dimensional supersonic viscous marching solver; the MINT code (refs. 6 to 16) as a general inviscid/viscous elliptic flow solver; and the PEPSIG code (refs. 17 to 21) as a generalized subsonic three-dimensional viscous marching flow solver for diffuser ducts. The PEPSI/MINT series of viscous flow solvers are "general" because the geometry, computational mesh along with all the necessary metric information, and the boundary conditions are external to the solution generator, i.e., this information must be supplied as input data.

Each of these three-dimensional flow field solvers has proven to be a successful technique for solving the set of equations at relevant flow conditions in relevant geometric configurations. They represent efficient and accurate methods for analyzing advanced supersonic inlet systems. In particular, the PEPSI/MINT series of general three-dimensional flow solvers was written in modular form so that changes in items such as boundary conditions, turbulence models, and geometry as well as additional terms representing new physical phenomena can be made in a straight forward manner. Changing one component, such as geometry or form of the governing equations, would not require changes in other parts of the code, such as the subroutines which solve the sets of equations. The PEPSI/MINT series of generalized flow solvers has been designed to provide the maximum flexibility to anticipate future needs and respond to those needs. Analysis of new configurations will thus focus upon the development of the geometry and mesh and in developing smoothness criteria for the particular flow algorithm and fluid dynamic characterists of the flow itself. Since these three-dimensional flow field codes have been extensively verified for a selected set of relevant benchmark experimental data (refs. 22 to 53) they represent the general set of spatial marching and elliptic solvers which forms the basis for ongoing and future computational efforts.

BENCHMARK VALIDATION AND IMPROVEMENT

The goal of providing design analyses tools for supersonic inlet system technology advancement necessitates a two tier experimental validation process to properly evaluate the ability of these three-dimensional solvers to predict the relevant flow physics. First, it is necessary to show good predictions of flow parameters of interest to the user community on "generic" configurations which would be typical of real world designs. Such testing should be as realistic as possible. Confidence in the advanced computational capability would increase by leaps and bounds in the user community by this type of demonstration.

A second tier program appears to be called for and here essential elements of these advanced computer design tools would be validated in very simple environments that highlight one or more basic flow mechanisms. The requirements are for overall simplicity and easy access to make the necessary very detailed measurements. Detil validataion of basic flow mechanisms is required because the generic component tests may or may not emphasize any particular basic flow mechanism and overall good agreement may be just that, an "overall" agreement. There may be an unfortunate cancelling effect in the basic flow mechanisms of generic experiments. For instance, one could not analytically investigate the factors affecting inlet performance with any degree of confidence if the individual shock wave turbulent boundary layer interactions encountered within the inlet were not well predicted (fig. 2). Confidence in

making extrapolations using computational tools will increase if the basic mechanisms, when isolated, are predicted both qualitatively and quantitatively.

The PEPSI/MINT series of general flow field solvers are large, complex, computer analyses designed to solve the three-dimensional flow field characteristic of advanced aircraft inlet concepts. As a result, benchmark validation and generic verification of these codes is a very important part of the program at NASA Lewis Research Center. A series of experimental data sets have thus been identified from the literature or obtained through university contracts or grants as well as inhouse experiments to be compared with the PEPSI/MINT codes.

Three-Dimensional Supersonic Viscous Marching Flow Solver (PEPSIS)

Following this philosophy on computer code validation, a series of generic inlet configurations have been identified from reports published and have been analyzed using the PEPSIS three-dimensional viscous flow solver. These supersonic inlets include the Mach 2.5 mixed compression inlet of Fukuda, Hingst and Reshotko (ref. 22) the Mach 3.0 mixed compression two-dimensional inlet of Anderson and Wong (ref. 23) the Mach 3.5 mixed axisymmetric inlet of Syberg and Hickcox (ref. 24) and the Mach 7.5 hypersonic inlet of Gnos and Watson (ref. 25). It was concluded in this series of generic inlet verification calculations that "overall" good agreement between experiment and analysis was achieved although a great deal of uncertainty exsisted in understanding the details of the bleed interaction. This uncertainty centered around five main points; namely (1) the bleed distribution through the bleed region was unknown, (2) the size of the bleed holes was often large in comparison to the boundary layer thickness, (3) the bleed mass flow was often large in comparison to the boundary layer mass flow approaching the bleed region, (4) the possibility that recirculation exsisted in the bleed region, and (5) transpiration took place using discrete holes rather than continuous bleed. As a result, a major benchmark bleed program was initiated at Lewis Research Center to obtain the necessary experimental data and physical understanding of the boundary layer bleed process.

In addition to this set of calculations on generic supersonic inlet configurations, a series of benchmark supersonic flow phenomenon has been identified and are presented in figure 3. These interactions include the oblique shock wave turbulent boundary layer interaction of Rose (ref. 26) the three-dimensional glancing sidewall shock wave turbulent boundary layer interaction of Oskam, Vas, and Bogdonoff (refs. 27 to 29) and the cone-at-alpha interaction of Rainbird (ref. 30).

Two-dimensional oblique shock wave interaction. - The first benchmark test case is that of the oblique shock wave turbulent boundary layer interaction studied by Rose (ref. 26). The oblique shock was generated by a 10° cone placed in a blow down circular tunnel operating at Mach 3.88 and Reynolds number of 5.0E6 per ft. In this calculation, the entire tunnel was modeled using a computation mesh of 89X450 (40 500 nodal points) with approximately 30 points in the boundary layer. On the Lewis CRAY I computer, this benchmark test case took 0.9 min of CPU time. A comparison of the calculated and experimental wall static distribution through the interaction zone is presented in figure 4 and demonstrates that the PEPSIS solver correctly predicts the two

4

stage measured static pressure generated by the oblique shock wave interaction
with the boundary layer. The abrupt initial static pressure was generated by
the impingement of the incident shock wave, and the more gradual downstream
static pressure rise was caused by the formation of the reflected shock system.
Figure 5 presents the comparison between the calculated and measured Mach num-
ber profiles through the interaction zone. The incident shock appears as a
discontinuity in the experimental data, while shock smearing occurs over sev-
eral grid points. The PEPSIS analysis predicts well the development of the
Mach number profiles including the thinning of the boundary layer. A detailed
discussion concerning the manner in which this calculatiuon was performed
appears in a paper by Benson and Anderson (ref. 37).

Three-dimensional glancing sidewall interaction. - A schematic diagram
depicting the analytical and experimental test configuration used to study the
glancing sidewall turbulent boundary layer interaction is shown in figure 6.
This interaction arises when the oblique shock wave formed by the wedge inter-
acts with the wall boundary layer. Because of the skewing of the incident
shock wave across the boundary layer on the tunnel wall, a strong transverse
static pressure gradient is established which generates strong cross flows.
The nominal Mach number upsream of the wedge was 2.84, the tunnel total pres-
sure was set at 88.9 psia and the tunnel free stream total temperature was
445.0° Rankine. Two computational mesh systems were used to study the glanc-
ing sidewall boundary layer interaction, a coarse grid composed of 40X40X100
(160 000) nodal points and a medium grid with 40X60X90 (216 000) points. On
the Lewis CRAY I high speed computer, these calculations were accomplished
using 6.0 and 9.6 min of CPU time, respectively. Shown in figures 6(a) to (c)
is a comparison of the computed and measured yaw angle distribution through
the wall boundary layer. The yaw angle is defined as the ratio of the velocity
in the YG-direction which is parallel to the tunnel sidewall, divided by the
velocity in the X-direction. This is a particularly difficult parameter to
calculate since it represents the ratio of two velocities which approach zero
as the wall is approached. It is apparent that very good agreement was ob-
tained using the PEPSIS analysis to model this important interaction. A detail
study into the effect of wall functions and mesh resolution was performed by
Anderson and Benson (ref. 36) with the conclusion that insufficient mesh reso-
lution of the near wall region caused discrepancies to appear in the calcula-
tion of the velocity field.

A detail picture of the flow field in the tunnel sidewall region is shown
in figure 7. In the vicinity of the tunnel sidewall, a very strong vortex is
established which elongates and increases in strength in the downstream direc-
tion. This causes very low energy flow to accumulate in the corner region
with resulting low wall shear stress in this region. This probably accounts
for the very high heating rates measured by Oskam, Vas and Bogdonoff (refs. 27
to 29). The increased strength of the sidewall vortex is also suggested by
the experimental data results since the maximum yaw angle increases in the
downstream direction. The oveturning that occurs in the sidewall boundary
layer results from an imposition of the main stream static pressure gradient
upon the low momentum near wall viscous flow. This overturning results in low
energy fluid being drawn in towards the tunnel sidewall in the lower ramp
region. In the outer ramp region, the flow rolls over to form the sidewall
vortex. As the flow develops in the downstream direction, the sidewall vortex
losses its identity and the surface velocity vectors tend to align themselves
with the shock angle.

Figure 8 presents the static pressure signature calculated on the ramp and tunnel sidewall surfaces. The numerical formation of the shock wave in the region of wedge tip can clearly be observed as well as the shock wave formation on the tunnel sidewall surface. Although not explicitly shown in figure 8, an adverse static pressure gradient exsist in the near wall region of the wedge and tunnel sidewall surfaces. Of special interest is the fact that static pressure gradients are established on the ramp surface as a result of the corner flow boundary layer development. The static pressure gradients that are created on the ramp and tunnel sidewall surfaces fall inside a conical region of influence.

The global features of the glancing side interaction that emerge from this study can be viewed as two separate flow regions, namely a large outer region of inviscid high energy flow which follows the inviscid stream lines, and a smaller inner region near the wall composed of low energy fluid which migrates along the shock wave. The low energy flow will eventually accumulate in the corner region of the tunnel ceiling causing severe problems. This flow is called the glancing sidewall/corner shock wave turbulent boundary layer interaction and will be discussed later in this paper.

Cone-at-alpha interaction. - To understand the importance of adequate mesh resolution in critical computational regions, a series of calculations were performed using the experimental configuration of Rainbird (ref. 30). This experiment consisted of a 12.5° half angle cone mounted in the supersonic wind tunnel at 15.6° angle of attack. The Mach number for this series of calculations was set at mach 4.25. The extreme angle of attack conditions were chosen because a recirculation vortex developes as a result of the interaction of the windward and leaward boundary layers.

Figure 9 demonstrates the importance of radial and circumferential mesh resolution for this problem. The figure shows Mach number contours for the aft quadrant of the flow field for different meshes at a plane near the measuring station. All of the calculations required 220 streamwise stations, with nearly 100 of them located near the cone tip to resolve the formation of the shock. Figure 9(a) shows the results of the first calculation with 49 radial points packed near the cone surface, and 19 circumferential points evenly spaced at every 10°. The results indicate a thickening of the boundary layer on the leeward side, and give no indication of a recirculation. Increasing the number of circumferential points to 37 evenly spaced at 5° while maintaining 40 radial points gives the results of figure 9(b). This calculation gives an indication of recirculation but with little detail. Because the recirculation is caused by interactions in the boundary layer, more resolution was required in the radial direction near the surface. Packing the 49 radial points closer to the surface gave the results shown in figure 9(c). While resolving details of the surface, resolution of the shock wave was sacrificed which resulted in violent post shock pressure oscillations. To resolve both the shock and the boundary layer, the radial mesh was increased to 80 points. The results shown in figure 9(d) indicate that the calculation was then able to resolve boundary layer details without oscillations near the shock wave. Figure 9(e) shows one further refinement in which the circumferential mesh was increased to 50 points which were packed on both the windward and the leeward rays. The marked difference in the results of figure 9(a) and figure 9(e) clearly demonstrates the need to resolve all of the small and large scale phenomena present in this problem. The 40X19X220 (167 000) mesh point calculation used 6.0 min of CPU

time on the Lewis CRAY I high speed computer, while the 80X50X220 (880 000) nodal point calculation used 31.7 min of CPU time. Figure 10 shows the computed recirculation vortex which formed on the leeward side of the cone flow field in terms of the secondary velocity vectors for the 80X50 transverse mesh system. Note the overshoot in the circumfrential velocity in the region to the waterline side of the the recirculation vortex.

In addition to these benchmark interactions, a major experimental program is underway at the NASA Lewis Research Center to obtain detail data on selected two and three-dimensional shock wave boundary layer interactions which focuses on the details of boundary layer bleed (fig. 11). Recent efforts to benchmark validate the PEPSIS flow solver have been directed towards understanding the details of these bleed interactions and improving the bleed model to accurately describe the flow physics of this interaction. Data obtained by Hingst and Tanji (ref. 31) in the Lewis 1x1 Supersonic Wind Tunnel is being used as the benchmark standard since detail boundary layer profile through the interaction and bleed flow distribution through the holes were measured. Along with the shock wave boundary layer bleed interaction study, the glancing sidewall/corner shock wave interaction, previously mentioned, is also being examined experimentally in the 1X1 ft Supersonic Wind Tunnel.

Glancing sidewall/corner interaction. - Figures 12 and 13 present the analytical and experimental oil flow patterns resulting from the the impingement of the glancing sidewall flow field with the tunnel floor of the 1X1 ft Lewis Supersonic Wind Tunnel. The mesh system used to study the glancing sidewall/corner interaction was composed of 80X40X120 (384 000) grid points. Calculations were performed on the Lewis CRAY I computer using 14.4 min of CPU time. Although the shock static pressure rise was not sufficient to separate the flow in the analysis on the center portion of the tunnel floor, there is a corner region separation that was revealed in the calculations and can be seen in the experimental oil flow patterns. Because this interaction is typical of a class of problem corner interaction that can be found in the advanced supersonic inlets concepts, it was deemed important to obtain detailed experimental benchmark data in the Lewis 1X1 ft Supersonic Wind Tunnel.

The PEPSIS three-dimensional viscous analysis is also being used to identify selected benchmark phenomenon that will become important in the design of advanced aircraft inlet concepts (fig. 14). These highly three-dimensional shock wave turbulent boundary layer interactions center around the hypersonic corners interaction of Cresci (ref. 32) the intersecting wedge interaction of West and Korkegi (ref. 33) and the skewed wedge interaction of Settles, Perkins, and Bogdonoff (ref. 34) and the crossed side shock wave turbulent boundary layer interaction for which no benchmark data is available.

Hypersonic corner interaction. - The primary interest in the experiment by Cresci (ref. 32) was directed towards the hypersonic, low density flow regime wherein the inviscid shock layer and the viscous boundary layer produced under these conditions are of the same order of magnitude. In this case, the viscous and inviscid effects are interrelated and cannot be treated independently. This phenomena is important in that it represents a complex corner interaction that is typical of a large class of problems associated with advanced supersonic inlet concepts. The structure of the corner flow interaction is shown in figure 15. Qualitatively, the structure is similar to that found by West and Korkegi (ref. 33) and consists of an oblique corner shock

resulting from the intersection of the shock waves generated by the rapid boundary layer growth on the wall surfaces, and a set of two tripple points formed by intersection of the embedded shock wave system. This interaction was studied by Buggeln, McDonald and Kin (ref. 5) using the PEPSIS forward marching three-dimensional flow solver, as part of the benchmark verification process. The model was mounted in a Mach 11.8 blowdown wind tunnel, and tests were conducted at free stream Reynolds varying between 0.15E6 and 0.5E6. The tunnel stagnation temperature varied between 1700° Rankine and 1900° Rankine which produced wall temperature ratios of 0.29 and 0.32. Calculations were performed on the hypersonic corner interaction using a grid system composed of 50X50X120 (300 000) nodal points. Although the calculations were performed on the Lewis IBM 370/3033, the equivalent computing time on the Lewis CRAY I computer would be 10.8 CPU min. Figures 16 and 17 present the calculated Mach number and total pressure field of the hypersonic corner interaction. The primary features of an oblique corner shock wave generated by the intersection of the the boundary layer shock wave from the wall surfaces and the set of tripple points formed by the embedded shock system are easily seen in these figures. In addition, the secondary feature of a triangular region bounded by two slip surfaces and the corner shock wave was also revealed in the calculations.

Lewis 40/60 mixed compression inlet. - Figures 18 through 20 present a series of calculations on a Mach 2.5 mixed compression supersonic inlet at 0° and 2° angle of attack. The purpose of the study was threefold, namely (1) to examine the problems associated with computing boundary layer bleed within an inlet enviorment, (2) to study the effects of boundary layer bleed on inlet characteristics, and (3) to anticipate flow problems associated with the three-dimensional shock boundary layer interactions of this inlet at angle of attack and recommend solutions. A detailed experimental bleed study was performed on this inlet by Fukuda, Hingst and Reshotko (ref. 22) in the 10X10 Supersonic Wind Tunnel at Lewis Research Center. This axisymmetric mixed compression inlet was designed for a Mach number of 2.5 with 40 percent external area contraction and 60 percent internal contraction. The external compression was accomplished with a 12.5° half angle cone and the internal cowl lip angle was 0.0°. Figure 18 presents the results of a two-dimensional calculation using wall functions to establish a baseline or reference case. The two-dimensional computational mesh was composed of 89 radial points and 360 forward marching steps for a total of 32 040 nodal points. On the Lewis CRAY I high speed computer, this calculation used 0.7 CPU min. Shown in figure 18 are the local Mach number profiles computed within the inlet geometry. The cone shock as well as the reflected shock system within the inlet are clearly visable. The cowling produced an internal shock wave system which reflected first off the centerbody and then off cowling reaching the throat region for a second centerbody interaction. The second centerbody reflected shock was the terminal shock when the model was operated in the critical mode.

As an initial start to examine the three-dimensional shock wave turbulent boundary layer interactions that can arise within axisymmetric inlets at angle of attack, two separate cases were considered using the PEPSIS three-dimensional flow solver. In the first case, the 40-60 inlet was operating at the design Mach 2.5 condition and 2.0° angle of attack, and in the second case, the 40-60 inlet was operating at Mach 3.0 condition, also at 2.0° angle of attack. In each case, the centerbody was in the design position for zero angle of attack operation. The design Mach number calculation revealed a large

8

region of subsonic flow on the leaward side of the first cowl reflection.
This is in subtantial agreement with limited experimental data at this condi-
tion. Since little information could be obtained on the three-dimensional
character of the shock wave turbulent boundary layer interactions within this
inlet for the first case, the overspeed case was run.

The Mach 3.0 angle of attack case used a computational mesh composed of
49X19 nodal points in the transverse plane and 480 forward marching step for a
total of 446 880 grid points. The computing time for this case was 16.9 CPU
min on the Lewis CRAY I high speed computer. Figures 19 and 20 present the
results of this calculation. For the inlet operating at the design Mach number
and at 0° angle of attack, the cone shock is located just outside the cowl
lip, thus spilling about 0.5 percent over the cowl. In the Mach 3.0 overspeed
case, the cone shock is forced inside the cowl lip. At angle of attack, this
shock system translates forward on the leeward side and rearward on the wind-
ward side, thus creating a small expansion region on the cowl lip. Figure 19
shows surface static pressure distribution on the cowl and cone. The shock
waves are clearly shown as light bands which are inclined relative to the inlet
axis. On the cone, the shock system moved forward on the leeward side and aft
on the windward side, while on the cowl, the first rather weak shock from the
cone tip and the stronger shock from the cone reflection are clearly evident.
Also evident on the inlet surfaces are pressure contours which are normal to
the inlet axis, particularly near the throat section on the cone and along the
cowl between the shocks. These features are the results of compressions and
expansions present in the inlet due to surface contouring. For an other per-
spective of this flow field, static pressure and Mach number contours in the
flowfield at the windward, waterline, and leeward rays are presented in
figure 20. On the windward ray, the cone shock fall inside the cowl lip, while
on the leeward ray, the cone shock falls forward of the lip. The static pres-
sure again indicates the proper shock translation with the leeward shock mov-
ing forward and becomming stronger than the windward interaction. Also evident
are the expansions near the throat and its interaction with the shock system.
The Mach number contours indicate this same behavior, but also shows the bound-
ary layer variations through the calculation. Work is continuing on these
three-dimensional shock wave boundary layer interactions.

Three-Dimensional Elliptic Inviscid/Viscous Flow Solver (MINT)

Specification of high grid resolution in the vicinity of a no-slip wall
is obviously required to resolve the wall boundary layers. However, specifi-
cation of a high resolution region to resolve a normal shock wave is not a
simple problem because the shock location and shape may not be known a priori.
Thus, a viable shock tracking adaptive mesh strategy was developed to properly
resolve the regions of high gradients for normal shock wave turbulent boundary
layer interactions. In particular, a search for the maximum pressure gradient
location was used to establish a definition for the shock wave center. Since
any spurious oscillations in the solution could prove detrimental to accurate
shock center determination, a "filtering scheme" was applied to the process of
the shock location. Essentially, the procedure identifies turning points in
the wall static pressure distribution, examines the change in pressure between
subsequent turning points and carries out a search for the maximum pressure
gradient in the interval having the largest pressure rise. Once the shock
center is located, a new grid is constructed by centering a sinh function at

the new shock center location. The grid motion is accounted for in the governing equations through inclusion of terms containing derivatives of the computational coordinates with time.

The present effort to benchmark verify the MINT general inviscid/viscous three-dimensional flow solver (fig. 21) has centered around the normal shock turbulent boundary layer interaction in the channel of Mateer and Viegas (ref. 38) and in the variable area diffuser of Sajben, Bogar, and Kroutil (ref. 41). In particular, two main issues were under investigation, namely, (1) does an adaptive mesh or grid clustering region which moves with the shock region during the course of the calculation introduce any significant errors, and (2) what role does artificial dissipation play in solution accuracy.

Constant area two-dimensional normal shock wave interaction. - The first case considered simulates the normal shock wave turbulent boundary layer interaction which will occure at modest upstream supersonic Mach numbers in a constant area tube with circular cross section. The case has been specified to match the experimental data of Mateer and Viegas (ref. 13). The calculation was performed for an inlet Mach number of 1.44, an imposed exit to inlet static pressure ratio of 2.0, and a Reynolds number of 5.83E5 based on upstream boundary layer thickness of 2.5 centimeters. In order to maintain adequate mesh resolution in all parts of the flow field, the adaptive mesh strategy described earlier was invoked. The calculation was performed on a computational mesh with 41 transverse and 31 streamwise points, using a mixing length turbulence model. In the original analysis paper by Roscoe, Shamroth, Gibeling, and McDonald (ref. 13) comparison between experimental data and analysis were made with both a mixing length and k-e turbulence model. The results obtained with the mixing length turbulence are shown in figures 22 and 23. Figure 22 presents a comparison between the measured and calculated static pressure distribution while figure 23 presents the comparisions for the streamwise velocity profiles through the interaction region. It is apparent that the mean flow quantities are well predicted by this method and the adaptive mesh strategy described introduced no appreciable error in the calculation.

Variable area two-dimensional normal shock wave interaction. - Figures 24(a) and (b) present a comparision between MINT Navier Stokes calculations of the normal shock wave turbulent boundary layer interaction in a variable area diffuser with the experimental data of Sajben, Bogar, and Kroutil. Calculations were performed on a computational mesh consisting of 25 streamwise points and 25 transvers nodal points. The computations were performed on the Lewis IBM 370/3033 high speed computer, and required 0.013 CPU secs per grid point per time step. Since that calculation, the computing time has been reduced to 0.0065 CPU secs per grid point per time step as a result of code "clean-up". The equivelant time on the Lewis CRAY I high speed computer would therefore be 6.5E-4 CPU secs per grid point per time step after vectorization. The calculated top wall distribution is shown in figure 24(a) and the calculated bottom wall distribution is shown in figure 24(b). Solutions were obtained with two values of artificial dissipation, $\sigma = 0.05$ and $\sigma = 0.5$. It is obvious that the choice of the artifical dissipation parameter significantly affects the calculated results. The normal shock is captured properly with $\sigma = 0.05$, while the results were severlly smeared with $\sigma = 0.5$. In fact, the $\sigma = 0.5$ calculations did not even contain a supersonic region (fig. 24).

The excellent results obtained using the MINT three-dimensional flow solver established clearly that an adaptive grid approach can be used to

10

calculate shocked flow fields in which the position of the shock wave is un-
known a priori. Also, the role of the artificial dissipation parameter was
examined in this study. For an inappropriate choice of artifical dissipation,
the solution will be severlly smeared and may, in fact, even suppress the
appearance of the terminal shock region. A detailed discussion concerning the
manner in which these calculations were performed as well as a more in depth
examination of the effects of artifical dissipation appear in two publications
by Liu, Shamroth, and McDonald (refs. 14 and 15). Future investigation on the
normal shock wave turbulent boundary layer interaction will center on the
problems conserning the responce of the terminal shock to an externally applied
disturbance and the effects of turbulence modeling on the small scale flow
properties. Early efforts to understand the dynamic effects of a back pressure
disturbance on the normal shock wave turbulent boundary layer interaction
appears in a paper by Liu, Shamroth, and McDonald (ref. 16).

Three-Dimensional Subsonic Viscous Marching Flow Solver (PEPSIG)

     Recent effort to benchmark the PEPSIG general three-dimensional subsonic
viscous marching flow solver has centered around the development of secondary
flow in a number of subsonic duct configurations (fig. 25). The philosophy
underlying this list of benchmark phenomena was to verify the PEPSIG three-
dimensional flow field solver on a sequence of flows with increasing complex-
ity. These include laminar and turbulent flow in a 90° bend with a square
cross section of Taylor, Whitelaw, and Yianneskis (ref. 44) laminar and tur-
bulent flow in the 90° bend with circular cross section of Enayet, Gibson, and
Taylor (ref. 45) laminar flow in the 180° circular pipe of Agrawal, Talbot,
and Gong (ref. 46) laminar and turbulent flow in the S-shaped ducts with square
and circular cross sections of Taylor, Whitelaw, and Yianneskis (refs. 47 and
48) the turbulent flow in the 45-45 circular S-shaped duct of Bansod and
Bradshaw (ref. 49) and the turbulent flow in the square-to-round transition
duct of Taylor, Whitelaw, and Yianneskis (ref. 50). In addition, NASA Lewis
also is sponsoring an experimental effort at the University of Tennessee Space
Institute to study the structure of secondary flows in S-ducts with high
entrance Mach number and diffusion. Experimental results of this effort appear
in a paper by Vakili, Wu, Bhat, Liver, Hingst, and Towne (ref. 51).

     Circular 90° Bend. - Extensive calculations were made for the flow geom-
etry in which detailed measurements were made by Enayet, Gibson, and Taylor
(ref. 45). This geometry consisted of a circular duct with a 90° circular-
arc-bend and with straight sections both upstream and downstream of the bend.
The ratio of bend radius to duct width was 2.3. The measurements were taken
for Reynolds number of 790 (laminar flow) and 40 000 (turbulent flow). Two
computational grid systems were used for the laminar evaluation; a coarse mesh
system composed of 20X20X75 (30 000) nodal points and a fine grid system com-
posed of 40X40X75 (120 000) points. On the Lewis CRAY I high speed computer,
these two cases used 0.7 and 2.9 min of CPU time. Likewise, two grid systems
were also used to evaluate the turbulent data; a coarse mesh composed of
25X25X86 (53 750) points and a fine mesh system having 50X50X86 (215 000) nodal
points. Calculations were performed on the Lewis CRAY I computer using a total
of 1.3 and 5.1 min of CPU time respectively. A comparison between the experi-
mental data and the analysis using the coarse and fine grid system is pre-
sented in figure 26 for the laminar flow case. Two regions of separation were
encountered for the laminar flow case. The first separation region was

located at the entrance to the bend on the outer wall and the second on the inner wall near the bend exit. A comparison of the measured and computed streamwise velocity profiles (fig. 26) show that the "separation model" within the PEPSIG flow solver can simulate the effects of "weak" separations on the main flow field. Figure 27 presents the structure of the secondary flow at the four experimental measuring stations. The secondary flow is formed because the fluid near the flow axis, having higher velocity, is acted upon by a larger centrifugal force than the slower fluid near the walls. The faster moving fluid at the center moves outwards, pushing the fluid in the boundary layer at the outer wall around towards the inner wall. Thus fresh fluid is continually being brought into the neighborhood of the outer wall and forced towards the inner wall. The overturning that occurs in the boundary layer generates a strong vortex system, which migrates away from the wall near the bend exit. Presented in figure 28 is a comparison between the measured and computed turbulent streamwise velocity profiles at the four measuring stations through the 90° bend. For turbulent flow, the results were very sensitive to mesh resolution in the regions of high shear, as can be seen in figure 28. Figure 29 presents the turbulent secondary flow structure which consists of a pair of counter-rotating vorticies formed from the overturning of the flow within the wall boundary layer. This "overturning" can also be seen in the surface oil film patterns presented in figure 29.

Circular 180° Bend. - Agrawal, Talbot, and Gong (ref. 46) have obtained detailed LDV measurements of laminar flow development in curved pipes with uniform entry velocity. This experimental data was used by Towne (ref. 53) to evaluate and verify the ability of the PEPSIG three-dimensional viscous flow solver to quantitatively predict the generation of pressure driven secondary flows in curved ducts. Experimental data was obtained at a Reynolds number of 1263, based on the cross sectional radius, and an entry velocity corresponding to a Dean number of 565. A computational mesh consisting of 50X50 nodal points in the transverse plane and 226 forward marching steps, for a total of 565 000 mesh points, was used for the results shown in figure 30. On the Lewis CRAY I computer, this calculation took 17 min of CPU time. A comparison between the measured and calculated streamwise contour plots presented in figure 30 demonstrate that for well prescribed geometry description and initial data, the PEPSIG flow solver can simulate the fine detail of flow structure associated with developing pressure driven flow fields.

Circular 22.5-22.5° S-Bend. - Taylor, Whitelaw and Yianneskis (ref. 48) in an experimental investigation sponsored by NASA Lewis Research Center, obtained a series of three-component LDV velocity measurements on the structure of the flow that develops in a 22.5-22.5° circular S-bend. Measurements include laminar flow at a Reynolds number of 790 and turbulent flow at a Reynolds number of 48 000. Two computational grid systems were used for the laminar evaluation; a coarse mesh system composed of 20X20X80 (32 000) nodal points and a fine grid system composed of 40X40X80 (128 000) points. On the Lewis CRAY I high speed computer, these two cases used 0.8 and 3.0 min of CPU time. Likewise, two grid systems were also used to evaluate the turbulent data; a coarse mesh composed of 25X25X80 (50 000) points and a fine mesh system having 50X50X80 (200 000) nodal points. Calculations were performed on the Lewis CRAY I computer using a total of 1.2 and and 4.8 min of CPU time respectively. Figure 31 presents a comparison between the measured and computed laminar development of streamwise velocity profiles at the four measurement stations through the S-duct. Because the boundary layers with this duct were large

12

relative to the duct dimensions, the laminar flow calculations were not sensitive to mesh resolution. The complex secondary flow structure that can develop in S-duct configurations is graphically shown in figure 32. The system of counter rotating vortex pairs develops in the first bend, and in the second bend, the secondary flow begins to reverse forming another pair of counter rotating vorticies. Also presented in figure 31 are the wall shear stress signatures that result from this secondary flow structure. Much greater sensitivity to resolution of high shear regions was encountered for the turbulent flow development through the S-duct (fig. 33). Qualitatively, the turbulent flow development resembles the laminar field; however, the high Reynolds number in the developing turbulent flow results in less severe secondary flow (fig. 31). Again, the computed results are in very good agreement with both the laminar and turbulent measurements (ref. 47).

Circular 45-45° S-Bend. - A series of measurements obtained at the Department of Aeronautics, Imperial College of Science and Technology, by Bansod and Bradshaw (ref 49) were used to verify the PEPSIG flow solver at higher Reynolds numbers. The configuration used for this study was the 45-45 symmetric short intake S-shaped duct with an R/D of 2.25. The duct entry velocity was nominally set at 45 meters/sec, which gave a Reynolds number of 5.0E5 based on duct diameter. Measurements were presented of total pressure, static pressure, surface shear stress, and yaw angle for the flow through the S-shaped duct. The computational mesh used for this study was 50X50X100, which gave a total number of grid points of 250 000. Computations were performed on the Lewis CRAY I high speed computer using 6.0 min of CPU time. Shown in figure 35 is a comparison between the calculated and measured surface shear stress at three circumferential surface lengths labeled the N-length, E-length, and S-length. Excellent agreement was obtained in spite of the fact that a simple eddy viscosity turbulent model was used in this calculation. Also shown in figure 35 is the surface shear stress color signature for this S-shaped duct. The small region of separation or near separation that was observed by Bansod and Bradshaw along the N-length is clearly visible from the wall shear stress signature. Figure 36 shows a comparison between the calculated and measured total pressure loss contours at the compressor face station in addition to the secondary velocity vector flow field. It is clear that the PEPSIG three-dimensional flow solver captured the proper flow physics at the compressor face including the pair of counter-rotating vortices in the boundary layer observed (ref. 49).

Square-to-round transition duct. - Included in the series of experiments sponsered by NASA Lewis Research Center at Imperial College of Science and Technology, London, was flow in a square-to-round transition duct. These results have been published by Taylor, Whitelaw and Yianneskis (ref. 50) and include three-component LDV measurements of the velocity field through the transition duct. The flow in this straight centerline transition duct was turbulent at a Reynolds number of 35 350. The computational mesh used for this calculation was 25X25 nodal points in the cross plane and 51 forward marching stations for a total number of 31 875 grid points. On the Lewis CRAY I computer, the CPU time was less than 1.0 min. Comparisons between the measured and calculated streamwise velocity profiles in a symmetry plane are presented in figure 37 at each reported measurement station through the transition duct. This comparison shows very good agreement between analysis and experiment.

13

Excellent results have been obtained using the PEPSIG three-dimensional viscous marching flow solver to model the development of pressure driven secondary flows, using a number of basic benchmark data sets for evaluation. Extensive evaluations were made for laminar flow within well defined duct geometries and well documented initial data. The excellent agreement with the laminar data demonstrates the accuracy of the solution algorithm without the uncertainty of describing the turbulent transport process by means of a turbulence model. This demonstration of accuracy should be a prerequisite to determining differences between numerics and physics, and in particular, the effects of turbulence model on solution results. In general, the flows studied were dominated by pressure forces rather than shear forces, hence, the influence of normal stress driven flows was small, and the effective viscosity approach was appropriate. Even with "weak" separations, the flows were primarily pressure controlled, although turbulent mixing became more important. Still, the effective viscosity approach may likely be the best compromise, but consideration should be given to stress turbulence models. These evaluations have established the importance of mesh point resolution in calculating the structure of secondary flow in subsonic diffusers, and consequently diffuser performance, compressor face recovery, and distortion. This presupposes that the duct geometry is well defined and computationally smooth, in addition to having an accurate description of the initial data.

Rockwell B1B inlet duct. - Figures 38 and 39 present the results of a series of calculations on the Rockwell B1B inlet duct using the PEPSIG three-dimensional viscous marching flow solver. The purpose of the computer study was twofold; namely (1) examine the difficulties associated with surface fitting a "real" inlet duct geometry and (2) determine the effects of geometry description on the accuracy of the solution. The Rockwell B1B inlet duct transitions from nearly rectangular cross-section at the inlet face to a circular cross-section at the compressor face, with a double S-bend insert between these two stations. The computations were initiated with an entrance Mach number of 0.5 and Reynolds number of 1.0E6 per ft. Calculations were performed with a computational mesh consisting of 50X50X100 (250 000) nodal points using 7.5 min of CPU time on the Lewis CRAY I computer. Shown in figure 38 is the computed static pressure signature on the inside surface of the B1B inlet duct along with the surface analytical oil film patterns. The surface oil film patterns highlight the over turning that results in the double S-bend insert portion of this inlet duct, which helps form the total pressure distortion presented in figure 39. The "quality" of this calculation depended very strongly on the ability to describe a computationally "smooth" inlet duct surface and to compress the mesh into regions of high shear. Complex surface geometries, such as the B1B inlet duct, are very difficult to describe computationally, and much time and effort had to be expended on this problem. However, care in constructing the geometry and mesh system in the initial steps of a duct analysis pays dividends later in the design-analysis process.

USER ORIENTED CODE DEVELOPMENT AND PROTOCOL STUDIES

The results of the comparisons between the PEPSI/MINT analysis and benchmark experimental data demonstrate a strong need to establish a computation protocol to insure the analytical results are reasonable and the desired information correct. Careful attention has been paid to those factors which could substantially affect solution accuracy. In particular, the need for

14

adequate mesh resolution in regions of high shear has been shown to be a critical factor affecting solution accuracy in many flow problems. Use of excessive artificial dissipation to suppress spatial oscillations in the solution has also been shown to suppress critical physics. Accurate and computationally "smooth" duct geometries along with well defined initial data are also critical factors affecting solution accuracy. Thus the results from benchmark validations of the PEPSI/MINT codes are being carefully considered to assess their meaning and implications with particular emphasis on sensitive controlling parameters. Based on these studies, formal "case running" protocols or structure for code application will be developed to guide the general user community.

Another primary item to be considered under this effort would focus upon the use of computer graphics in understanding the highly complex flows that develop within advanced supersonic inlet systems. The use of graphics in these areas has been under development for several years at Lewis Research Center including advanced techniques for visualizing complex three-dimensional flows in inlet, nozzle, and mixer flow fields using color graphical techniques (refs. 54 and 55).

THREE-DIMENSIONAL GRID GENERATION AND NUMERICAL TECHNIQUES

The computational mesh is one of three key factors that have a profound effect on the accuracy of the numerical solution; the other two factors being the numerical solution algorithm and the flow field itself. These factors cannot be separated. In each of the zonal regions within the inlet system, the construction of the computational grid is the key factor. However, the relevant physics to be studied in each of these propulsion components may require elliptic solutions, either Euler or Navier Stokes, for all or part of the flow field. In turn, the construction of the computational mesh cannot be performed independently of the available solution algorithm. There are no quantifiable criteria for generating acceptable finite-difference grids, including an assessment of grid smoothness, skewness and cell aspect ratio independently of the numerical solution obtained on the mesh. Lastly, if three-dimensional elliptic solutions are to become routinely used, even on advanced computers such as the CRAY, then major efforts are required to increase the computing speed and effectiveness of the solution algorithm.

In solving the equations of fluid dynamics by numerical means, two major problem areas are encountered. The first is three-dimensional mesh generation and the second is the algorithm by which the governing equations are processed to obtain a solution. Mesh generation involves three distinct processes, (1) the description of the bounding surfaces, (2) construction of the grid lattice within the bounding surfaces, and (3) the solution dependent adaptation or clustering of the grid lattice to accurately define the region of rapid solution variation. The numerical algorithm used to obtain the solution also involves three distinct processes, (1) replacement of the system of equations with a discrete representation, (2) stable and efficient solution advancement, and (3) data base management to control the flow of information to and from the numerical solution generator.

15

Three-Dimensional Mesh Generation

Description of bounding surfaces. - Looking at each of the three processes involved in mesh generation, it is noted that a considerable amount of literature has evolved on the fitting of surfaces for CAD/CAM and other applications. Much use of this existing literature could be made for fluid flow problems, but to date it has not been exploited. It is recommended that some effort be expended to review, assess, and explore the possible use of this existing technology in the fluid mechanics of three-dimensional mesh generation.

Construction of the grid lattice. - The construction of the grid lattice within and fitted to the bounding surface can be accomplished in several ways. Most notable, the grid lattice can be constructed numerically either as the solution to a partial differential equation or geometrically as a parameterization of the bounding surfaces. Either way, the grid lattice construction requires some trial and error on the part of the analyst and the range of configurations is often limited. Fundamental studies of both the aforementioned approaches to grid construction are required to understand and improve the accuracy, reliability, generality, and ease with which grids may be generated. Of particular note is the development of mesh smoothness criteria and parameters which influence this smoothness, leading ultimately to improved grids for fluid dynamics computations. Most importantly, while basic understanding can be obtained in one or two space dimensions, this investigation will emphasize three-dimensional grid generation for the type of fluid flow problems encountered in inlet, mixer, and nozzle components.

Adaptive mesh clustering. - Adaptive mesh clustering is a very powerful technique to effectively use a limited number of grid points to define the multiple length scales which can arise in fluid dynamic problems, such as boundary layer and inviscid core regions. In numerous problems, particularly in three-dimensional space, the location of the region requiring definition is not known a priori, but emerges as the solution develops. A transonic shock wave boundary layer interaction would be a case in point. For such problems, adaptive mesh clustering is a very powerful technique. Particularly in three dimensions, sufficient mesh resolution cannot be afforded without some mesh clustering and knowledge of the extreme solution variation. Solution dependent mesh adaptation can cause instability and great care is required to obtain stable, accurate, and, in some cases, optimal mesh clustering. Consequently, basic studies of the solution dependent mesh adaptation algorithms are required to understand and improve the stability, accuracy, distribution, and adaption process in three-dimensional space.

Numerical Algorithm Development

Higher order discrete representation. - In the numerical solution of multidimensional flow problems, particularly in three dimensions, a major limitation is the available computer memory. To the user this means that the total number of grid points in the computational space must be limited with a concomitant degradation in the solution accuracy. Conversely, when a desired level of accuracy is sought, in many instances the required number of spatial grid points needed to achieve that goal could be excessively large so as to make the calculation either impractical or extremely expensive. Hence, there is a great interest in minimizing the total number of grid points and accruing

the associated benefits which include reduction in computing time, a reduction in core requirements and a reduction of data transfer. All of these factors contribute to lower computing costs.

A method of achieving these desired benefits is the use of higher order spatial difference approximations. The replacement of the continuous system of equations by an accurate discrete representation is especially important in three-dimensional space. In one dimensional space it is known that a more accurate discrete representation of the governing equations can be obtained which results in a reduction in the number of grid lattice points required for an accurate solution. In multidimensional space, the required grid point density in one dimension is raised to the power of the space dimension. This raising to the power transforms the modest grid point savings in one dimensional space to impressive benefits in three-dimensional space. Thus more accurate higher order discretization schemes should be investigated from the view point of multidimensional use.

Solution advancement. - The second process, that of solution advancement, has two major problem categories; (1) time dependent or unsteady flows and (2) steady-state flow problems. Fluid flow problems that require the transients to be resolved, such as subcritical self-sustained oscillations (inlet buzz), introduce considerations which are not present if only a steady state solution is sought. The transients generally pose a hyperbolic problem in time which is further complicated if the flow is incompressible or at a very low Mach number. In addressing the problem of accurately and efficiently resolving the transients, the needs and limitations of three space dimensions must be kept in mind. Basic studies would be expected to lead to more robust and economical time dependent multidimensional solution algorithm for subsonic, transonic, and supersonic flows.

The steady state flow problem of interest poses an "elliptic" or "mixed" problem in which all the boundary conditions affect all or nearly all of the interior flow field. The problem is also nonlinear, thus some form of iteration may be required. This in many schemes is added to a basically iterative approach to solving the elliptic problem. This has led to the investigation of the "fast" iterative elliptic solvers for some problems and fast direct schemes for other more restrictive problems. The fast "iterative" schemes are more general and are applicable to the Navier Stokes equations, the "parabolized" Navier Stokes equations and the Euler equations and hence should be actively pursued. A number of schemes have shown considerable promise on single equations such as matrix pre-conditioning, relaxation parameter cycling and even mesh cycling (multi-grid techniques) and have demonstrated improvement in the rate of convergence to steady state solution. The role of convergence acceleration in systems of equations is presently not well understood and should be actively investigated.

Data base management. - The third consideration for the solution algorithm is the data base management aspects of the problem. Here the architecture of the computer itself enters from the point of view of the available memory, data transfer capability, and processor parallelism. The CRAY computer is fast becoming the industry standard for large scientific computing and consequently it is advocated that this type of computer be used to guide the data base management aspects of the problem. Vectorization of the solution algorithm should be examined, but also in view of the large arrays involved in

17

three-dimensional flow calculations, the algorithm data and data transfer needs should be considered. It is possible that a highly structured algorithm with local data requirements could out perform another algorithm on the CRAY simply by virture of modest storage data transfer requirements. Thus, the consideration of the solution algorithm and the computer architecture must be borne in mind when evaluating the relative efficiency of the various schemes.

CONCLUDING REMARKS

A general system of three-dimensional viscous marching and elliptic solvers called PEPSI/MINT has been developed at the NASA Lewis Research Center for the analysis and design of advanced technology supersonic inlet systems. Through a systematic and careful evaluation of these solvers by a two tier validation process involving generic verification and detailed benchmark validation data, the applicability and performance of these codes is being assessed and documented. From the benchmark validation process, a formalized protocol is being developed to assist the user in applying these three-dimensional flow solvers to insure reasonable correctness and to be able to distinguish between numerics and physics. In addition, an extensive library of plotting and three-dimensional graphical routines were developed to assist the user in understanding the very complex flow fields emerging as solutions from these solvers.

Major advances in computational fluid dynamics have emerged from this program, but significant problems remain and these are being addressed. In particular, future effort will be directed towards the development of improved three-dimensional grid generation, numerical methodology, and computer technology utilization. Likewise, the detailed benchmark validation of the PEPSI/MINT solvers will continue considering more complex flow fields.

APPENDIX - GENERALIZED THREE-DIMENSION FLOW SOLVERS

An extensive effort is currently underway to structure the PEPSI/MINT three-dimensional flow solvers described in this section, such that they have the ability to communicate with each other. This is in keeping with the philosophy of the zonal methodology concept. Common file storage for all dependent variables, identical formatted restart input/output files, uniform geometry methods for all PEPSI/MINT codes and common plot files, to interface with the extensive library of existing three-dimensional plotting and color graphical programs (refs. 54 and 55) are among the tasks being undertaken.

Three-Dimensional Supersonic Viscous Marching Flow Solver (PEPSIS)

The PEPSIS code that has been developed (refs. 1 to 5) solves the set of three-dimensional forward marching equations applicable to flow fields within supersonic inlets and nozzles of axisymmetric, two-dimensional or conformal geometries. The equations used in the analysis are based on the parabolized form of the three-dimensional, steady state, ensemble-averaged Navier Stokes equations. In the supersonic region of the core flow field, the required parabolizing assumption simply reduces to the neglect of the streamwise diffusion terms. In the flows anticipated for this region, streamwise diffusion is negligible and, therefore, the assumption is not restrictive. In the subsonic portion of the flow field, further assumptions are necessary to control the appearance of branching solutions. Suppression of branching and development of a stable forward marching procedure requires replacing the normal momentum equation in the subsonic region by the usual boundary layer approximation, which, for zerc curvature, sets the normal derivative to zero and for curved walls, allows for coordinate curvature effects. In addition, the wall tangency condition is applied to the entire subsonic region. This latter condition replaces the continuity condition at the sonic line by a specified flow direction. Since the subsonic region for most problems of practical interests is expected to be small, these approximations are not expected to have detremental effects in calculating inlet flow fields.

The PEPSIS three-dimensional flow field solver has been applied to a variety of two and three-dimensional flow problems at supersonic speeds in the absence of a major separation zone. The flow solver accepts a general orthogonal coordinate system through an external mesh generator which generates computational grid points in the given physical domain. Boundary conditions are set via input data flags. Among those available are function, first derivative, and second derivative of the velocity, density, and temperature, specification of static pressure with its derivatives, momentum equation, one-sided inviscid governing equations, Mach line extrapolation, and wall function formulation. Inclusion of the energy equation as well as its form and the choice of two or three dimensions and viscosity options are controlled via input data flags. The PEPSIS flow field solver has been validated through detailed comparison with a large variety of two and three-dimensional experimental flow fields (refs. 22 to 37).

Three-Dimensional Elliptic Invisicd/Viscious Flow Solver (MINT)

The approach being used within the inviscid/viscous MINT flow field solver applies the consistently split Linear Block Implicit (LBI) procedure (refs. 6

to 16) to the Navier Stokes equations. The method can be briefly outlined as follows: the governing equations are replaced by an implicit time difference approximation, optionally a backward difference or Crank-Nicolson scheme. Terms involving nonlinearities at the implicit time level are linearized by a Taylor series expansion in time about the solution at the known time level, and spatial difference approximations are introduced. The result is a system of multidimensional coupled, but linear, difference equations for the dependent variables at the unknown or implicit time level. To solve these difference equations, the Douglas-Gunn procedure (ref. 10) for generating Alternating Direction Implicit (ADI) schemes as perturbations of fundamental implicit difference schemes is introduced. This technique leads to systems of coupled linear difference equations having narrow banded matrix structure which can be solved efficiently by a standard block elimination method.

The MINT three-dimensional flow field elliptic solver accepts a very general coordinate system through input of the physical location of the computational grid points. Boundary conditions are set through input data flags. Among those available are function, first derivative and second derivative of the velocity, density and temperature, specification of static and total pressure or their derivatives, and one-sided governing equations. Inclusion of an energy equation as well as the choice of two or three dimensions and turbulence model are controlled via input data flags. Specification of very high Reynolds number along with implementation of proper boundary conditions would allow the elliptic solver to be applied to the Euler equations. Finally, output including flow field arrays and generation of plot files are also controlled via input data flags. The MINT flow solver has been validated through two and three-dimensional calculation of transonic diffuser flows with a terminal shock wave (refs. 33 to 37).

Three-Dimensional Subsonic Viscous Marching Flow Solver (PEPSIG)

The PEPSIG three-dimensional flow solver (refs. 17 to 21) is a general approach used for predicting subsonic flows in three-dimensional passages having little or no streamwise separation and is based on the primary-secondary velocity decomposition method of Briley and McDonald (ref. 16) for application to viscous subsonic flow in smoothly curved geometries. The objective of this approach is to introduce approximations which adequately represent essential physical features of interest and yet lead to governing equations which can be solved much more economically than Navier Stokes equations. In the present application, it is necessary to provide an adequate representation of primary flows, secondary flows, viscous effects, and their local interactions. An inviscid flow solution is first obtained for the geometry in question. The inviscid flow satisfies an elliptic governing equation requiring downstream boundary conditions and thus includes transverse variations in streamwise pressure gradients usually associated with flows in curved passages. This a priori pressure field is then used as an imposed criteria upon a set of equations which constitutes a well-posed initial-value problem in space. Solution of these equations leads to a prediction of both the velocity field and the corrected pressure field. When solved as an initial value problem, the technique provides a reduction in computational effort of one or more orders of magnitude over Navier Stokes equations.

20

The PEPSIG three-dimensional flow field solver is applicable to complex geometries having curved and twisted centerlines, variable cross-sectional areas, and shapes which require the use of nonorthogonal body fitted coordinate systems. Quantitative assessment of the method's predictions has been made by comparison with experimental data for a variety of geometries and fluid dynamic conditions (refs. 43 to 53).

REFERENCES

PEPSIS Computer Code Development

1. McDonald, H., and Briley, W. R., "Three-Dimensional Supersonic Flow of a Viscous or Inviscid Gas," Journal of Computational Physics, Vol. 19, October 1975, pp. 150-178,.

2. Buggeln, R. C., McDonald, H., Levy, R. and Kreskovsky, J. P., "Development of a Three-Dimensional Supersonic Inlet Flow Analysis," NASA CR-3218, 1980.

3. Buggeln, R. C., McDonald, H., Kreskovsky, J. P. and Levy, R., "Computation of Three-Dimensional Viscous Supersonic Flow in Inlets," AIAA Paper 80-0194, Jan. 1980.

4. Buggeln, R. C., McDonald, H. and Kin, Y. N., "Computation of Multi-Dimensional Viscous Supersonic Flow by Spatial Forward Marching," AIAA Paper 83-0177, Jan. 1983.

5. Buggeln, R. C., McDonald, H., and Kin, Y. W., "Computation of Multi-Dimensional Viscous Flow by Spatial Forward Marching," (NASA CR in preparation).

MINT Computer Code Development

6. Briley, W. R., and McDonald, H., "Solution of the Multidimensional Compressible Navier-Stokes Equations by a Generalized Implicit Method," Journal of Computational Physics, Vol. 24, Aug. 1977, pp. 372-397.

7. Briley, W. R., and McDonald, H., "On the Structure and Use of Linearized Block Implicit Schemes," Journal of Computational Physics, Vol. 34, Jan. 1980, pp. 54-73.

8. McDonald, H., and Briley, W. R., "Computational Fluid Dynamic Aspects of Internal Flows," AIAA Paper 79-1445, July 1979.

9. McDonald, H., Shamroth, S. J., and Briley, W. R., "Transonic-Flow with Viscous Effects," Transonic, Shock and Multidimensional Flows, edited by Academic Press, New York, 1982, pp. 219-240.

10. Douglas, J., and Gunn, J. E., "A General Formulation of Alternating Direction Methods Part I Parabolic and Hyperbolic Problems," Numerishe Mathematik, Vol. 6, 1964, pp. 428-453.

11. Briley, W. R., "Numerical Method for Predicting Three-Dimensional Steady Viscous Flow in Ducts," Journal of Computational Physics, Vol. 14, Jan. 1974, pp. 8-28.

12. Eiseman, P. R., McDonald, H. and Briley, W. R., "A Method for Computing Three-Dimensional Viscous Diffuser Flows," UARL Report R75-911737, July 1975.

13. Roscoe, D. V., Shamroth, S. J., Gibeling, H. J., and McDonald, H., Investigation of the Mechanism of Transonic Shock Wave/Boundary Layer Interactions Using a Navier-Stokes Analysis," SRA Report R83-930006-F, October 1983.

14. Liu, N. S., Shamroth, S. J., and McDonald, H., "Numerical Solution of the Navier-Stokes Equations for Compressible Turbulent Two/Three-Dimensional Flows in the Terminal Shock Region of an Inlet/Diffuser," AIAA Paper 83-1892, July 1983.

15. Liu, N. S., Shamroth, S. J., and McDonald, H., "Numerical Solution of the Navier-Stokes Equations for Compressible Turbulent Two/Three-Dimensional Flows in Terminal Shock Region of an Inlet/Diffuser," NASA-CR-3723, 1983.

16. Liu, N. S., Shamroth, S. J., and McDonald, H., "Dynamic Response of Shock Waves in 2-D Transonic Diffuser and Supersonic Inlets," (Report in preparation).

PEPSIG Computer Code Development

17. Briley, W. R., Kreskovsky, J. P., and McDonald, H., "Computation of Three-Dimensional Viscous Flow in Straight and Curved Passages," UTRC Report R76-911841-9, Aug. 1976.

18. Eiseman, P. R., Levy, R., McDonald, H., and Briley, W. R., "Development of a Three-Dimensional Turbulent Duct Flow Analysis," United Technologies Research Center, East Hartford, Conn., Nov. 1978. (NASA-CR-3029).

19. Levy, R., McDonald, H., Briley, W. R., and Kreskovsky, J. P., "A Three-Dimensional Turbulent Compressible Subsonic Duct Flow Analysis for Use with Constructed Coordinate Systems," Scientific Research Associates, Inc., Glastonbury, Conn., Apr. 1981 (NASA-CR-3389), April 1981.

20. Levy, R., Briley, W. R., and McDonald, H., "Viscous Primary/Secondary Flow Analysis for Use with Nonorthogonal Coordinate Systems," AIAA Paper 83-0556, Jan. 1983.

21. Briley, W. R., and McDonald, H., "Analysis and Computation of Viscous Subsonic Primary and Secondary Flows," AIAA Paper 79-1453, July 1979.

PEPSIS Benchmark Experiments and Verification

22. Fukuda, M. K., Hingst, W. G., and Reshotko, E., "Control of Shock-Wave Boundary Layer Interactions by Bleed in Supersonic Mixed Compression Inlets," Case Western Reserve Univ., Cleveland, OH., FTAS/TR-75-100, Aug. 1975 (NASA-CR-2595).

23. Anderson, W. E., and Wong, N. D., "Experimental Investigation of a Large Scale, Two-Dimensional, Mixed-Compression Inlet System - Performance at Design Conditions, M=3.0," NASA TM X-2016, 1970.

24. Syberg, J., and Hickcox, T. E., "Design of a Bleed System for a Mach 3.5 Inlet," Boeing Co., Seattle, Wash., D6-60168, Jan. 1973. (NASA-CR-2187).

23

25. Gnos, A. V., and Watson, E. C., "Investigation of Flow Fields within Large Scale Hypersonic Inlet Models," NASA TN D-7150, 1973.

26. Rose, W. C., "Behavior of a Compressible Turbulent Boundary Layer in a Shock-Wave-Induced Adverse Pressure Gradient," PhD Thesis, University of Washington, August 1972.

27. Oskam, B., Vas, I. E., and Bogdonoff, S. M., "Mach 3 Oblique Shock Wave/Turbulent Boundary Layer Interactions in Three-Dimensions," AIAA Paper 76-336, July 1976.

28. Oskam, B., Vas, I. E., and Bogdonoff, S. M., "Oblique Shock Wave/Turbulent Boundary Layer Interactions in Three-Dimensions at Mach 3.0," AFFDL-TR-76-48, Pt. I, June 1976.

29. Oskam, B., Vas, I. E. and Bogdonoff, S. M., "Oblique Shock Wave/Turbulent Boundary Layer Interactions in Three-Dimensions at Mach 3.0," AFFDL-TR-76-48, Pt. II, March 1978.

30. Rainbird, W. J., "Turbulent Boundary-Layer Growth and Separation on a Yawed Cone," AIAA Journal, Vol. 6, Dec. 1968, pp. 2410-2416.

31. Hinst, W. R., and Tanji, F. T., "Experimental Investigation of a Two-Dimensional Shock-Turbulent Boundary Layer Interaction with Bleed," AIAA Paper 83-0135, Jan. 1983.

32. Cresci, R. J., "Hypersonic Flow along Two Intersecting Planes," AFOSR 66-0500, Mar. 1966.

33. West, J. E., and Korkegi, R. H., "Supersonic Interaction in the Corner of Intersecting Wedges at High Reynolds Numbers," AIAA Journal, Vol 10, May 1972, pp 652-656.

34. Settles, G. S., Perkins, J. L., and Bogdonoff, S. M., "Upstream Influence Scaling of 2D & 3D Shock/Turbulent Boundary Layer Interactions at Compression Corners," AIAA Paper 81-0334, Jan. 1981.

35. Anderson, B. H., and Towne, C. E., "Numerical Simulation of Supersonic Inlets Using a Three-Dimensional Viscous Flow Analysis," AIAA Paper 80-0384, Jan. 1980.

36. Anderson, B. H., and Benson, T. J., "Numerical Solution to the Glancing Sidewall Oblique Shock Wave/Turbulent Boundary Layer Interaction in Three-Dimensions," AIAA Paper 83-0136, Jan. 1983.

37. Benson, T. J., and Anderson, B. H., "Validation of a Three-Dimensional Viscous Analysis of Axisymmetric Supersonic Inlet Flow Fields," AIAA Paper 83-0540, Jan. 1983.

MINT Benchmark Experiments and Verification

38. Mateer, G. G., and Viegas, J. R., "Effect of Mach and Reynolds Number on a Normal Shock-Wave/Turbulent Boundary Layer Interaction," AIAA Paper 79-1502, July 1979.

39. Bogar, T. J., Sajben, M., and Kroutil, J. C., "Characteristic Frequency and Length Scales in Transonic Diffuser Flow Oscillation," AIAA Paper 81-1291, June 1981.

40. Salmon, J. T., Bogar, T. J., and Sajben, M, "Laser Velocimeter Measurements in Unsteady, Separated, Transonic Diffuser Flows," AIAA Paper 81-1197, June 1981.

41. Sajben, M., Bogar, T. J., and Kroutil, J. C., "Forced Oscillation Experiments in Supercritical Diffuser Flows with Application to Ramjet Instabilities," AIAA Paper 81-1487, July 1981.

42. Briley, W. R., Buggeln, R. C., and McDonald, H., "Computation of Laminar and Turbulent Flow in 90 Degree Square Duct and Pipe Bends Using the Navier-Stokes Equations," SRA Report-R82-920009-F, Apr. 1982.

PEPSIG Benchmark Experiments and Verification

43. Rowe, M., "Measurements and Computations of Flow in Pipe Bends," Journal of Fluid Mechanics, Vol. 43, Oct. 1970, pp. 771-783.

44. Taylor, A. M. K. P., Whitelaw, J. H. and Yianneskis, M., "Measurement of Laminar and Turbulent Flow in a Curved Duct with Thin Inlet Boundary Layers," Imperial College of Science and Technology, London (England), FS-80-29, Jan. 1981 (NASA-CR-3367).

45. Enayet, M. M., Gibson, M. M., Taylor, A. M. K. P., and Yianneskis, M., "Laser Doppler Measurements of Laminar and Turbulent Flow in a Pipe Bend," Imperial College of Science and Technology, London (England), FS-81-19, May 1982, NASA-CR-3551.

46. Agrawal, Y., Talbot, L and Gong, K., "Laser Anemometer Study of Flow Development in Curved Circular Pipes," Journal of Fluid Mechanics, Vol. 85, Apr. 13, 1978, pp. 497-518.

47. Taylor, A. M. K. P., Whitelaw, J. H., and Yianneskis, M., "Developing Flow in S-Shaped Ducts, I-Square Cross Section Duct," Imperial College of Science and Technology, London (England), FS-81-22, May 1982, NASA-CR-3550.

48. Taylor, A. M. K. P., Whitelaw, J. H., and Yianneskis, M., "Developing Flow in S Shaped Ducts Part II: Circular Cross-Section Duct," (NASA CR in preparation).

49. Bansod, P., and Bradshaw, P., "The Flow in S-Shaed Ducts," Aeronautical Quarterly, Vol. 23, May 1972, pp 131-140, .

50. Taylor, A. M. K. P., Whitlaw, J. H., and Yianneskis, M., "Turbulent Flow in a Square-to Round Transition," Imperial College of Science and Technology, London (England), FS-80-30, July 1981, (NASA-CR-3447).

51. Vakili, A., Wu, J. M., Bhat, M. K., Liver, P., Hingst, W. R., and Towne, C. E., "Comparison of Experimental and Computational Compressible Flow in an S-Duct," AIAA Paper 84-0033, Jan. 1984.

52. Towne, C. E., and Anderson, B. H., "Numerical Simulation of Flows in Curved Diffuser with Cross-Sectional Transitioning Using a Three-Dimensional Viscous Analysis," AIAA Paper 81-0003, Jan. 1981.

53. Towne, C. E., "Computations of Viscous Flow in Curved Ducts and Comparison with Experimental Data," AIAA Paper 84-0531, Jan. 1984.

User Oriented Code Development and Protocol Studies

54. Anderson, B. H., Putt, C. W., and Giamati, C. C., "Application of Computer Generated Color Graphic Techniques to the Processing and Display of Three-Dimensional Fluid Dynamic Data," NASA TM-82658, Nov. 1981.

55. Anderson, B. H., Putt, C. W., and Giamati, C. C., "Fluid Dynamic Data-In Color and Three Dimensions," Mechanical Engineering, Vol. 104, Mar. 1982, pp. 30-35.
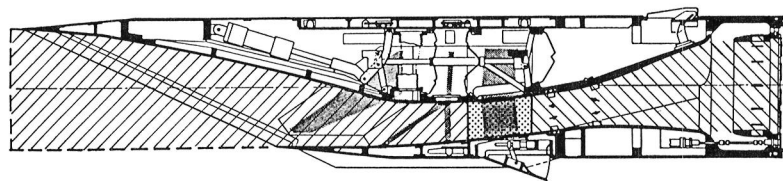
ANALYSIS		REGION
▨	3D SUPERSONIC VISCOUS MARCHING (PEPSIS)	INLET
▨	3D NAVIER STOKES (MINTZ)	TERMINAL SHOCK
▨	3D SUBSONIC VISCOUS MARCHING (PEPSIG)	DIFFUSER

Figure 1. – Supersonic inlet zonal methodology.
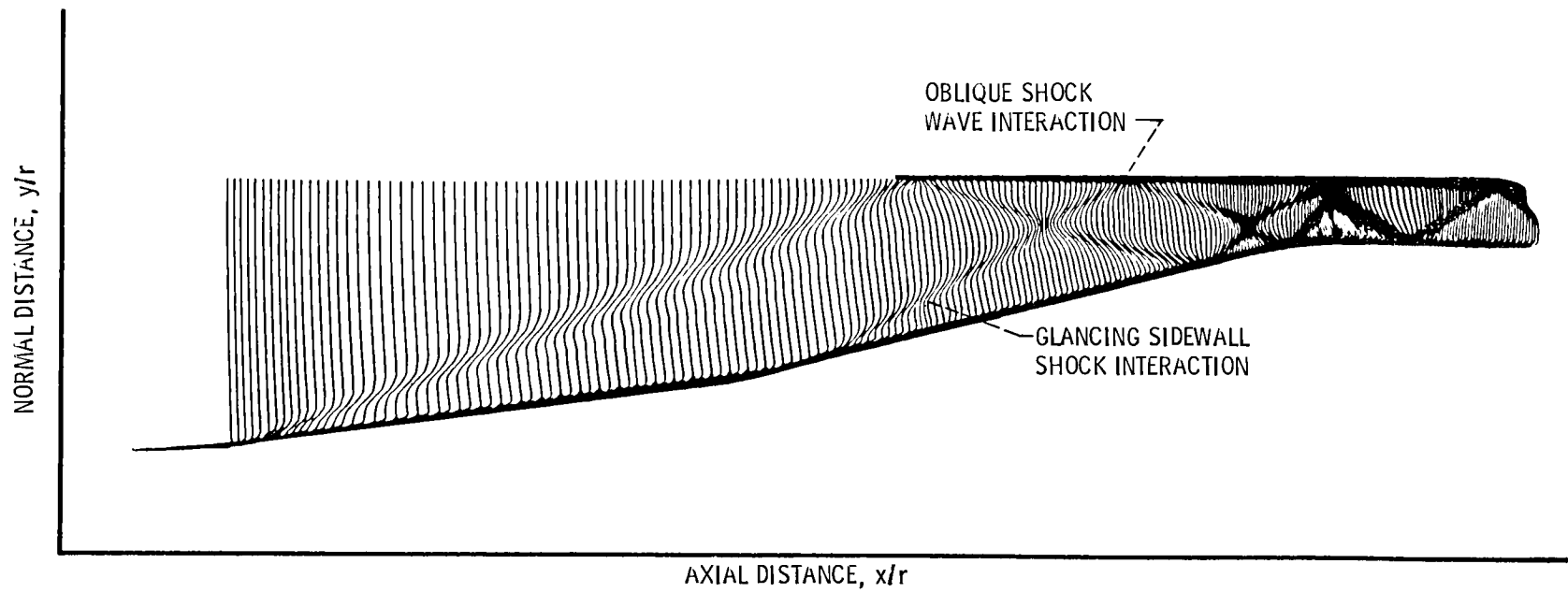
Figure 2 - Benchmark phenomenon.

PHENOMENON	SOURCE	TYPE OF DATA
● 2D SHOCK/BL/BLEED	LEWIS 40-60	LIMITED BL SURVEYS
	ROSE (AMES)	DETAIL BL SURVEYS (NO BLEED)
	1X1 LEWIS	DETAIL BL SURVEYS (BLEED RATES)
● 3D GLANCING SHOCK/ BL/BLEED	PRINCETON	DETAIL BL SURVEYS (NO BLEED)
	1X1 LEWIS	DETAIL BL SURVEYS (BLEED RATES)
● CONE AT ALPHA	RAINBIRD	LIMITED BL SURVEYS
● INLET AT ALPHA	10X10 LEWIS	DETAIL BL SURVEYS
● 3D CORNER SHOCK/BL	SHANG AND HANKEY	DETAIL BL SURVEYS

Figure 3. - PEPSIS benchmark verification.
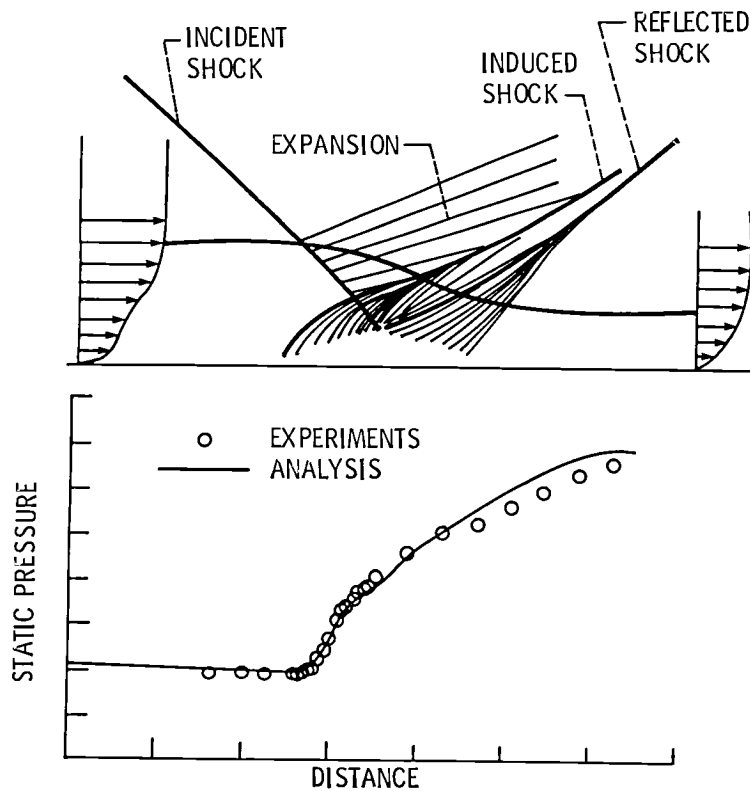
Figure 4. - Two dimensional oblique shock wave turbulent boundary layer interaction; static pressure distribution.
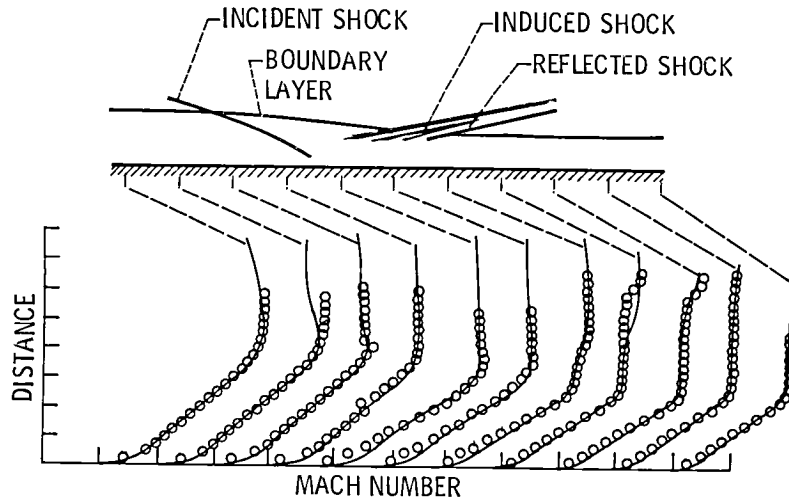
Figure 5. - Two dimensional oblique shock wave turbulent boundary layer interaction, Mach number profiles.
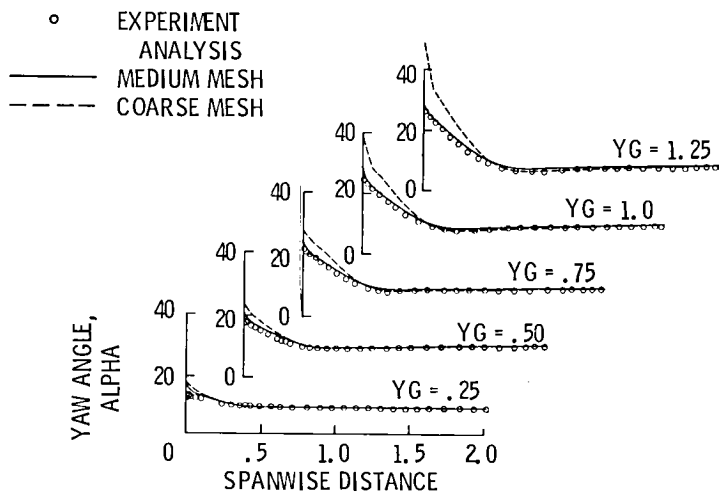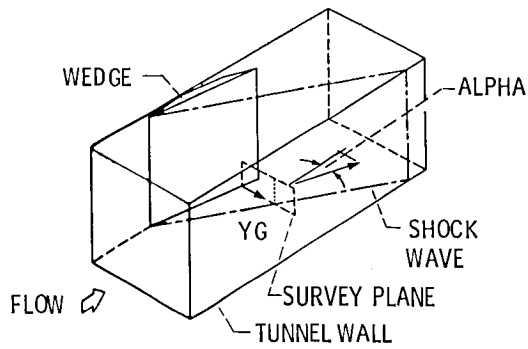
(a) Near wedge region.

Figure 6. - Three dimensional sidewall shock wave turbulent boundary layer interaction: yaw angle distributing.
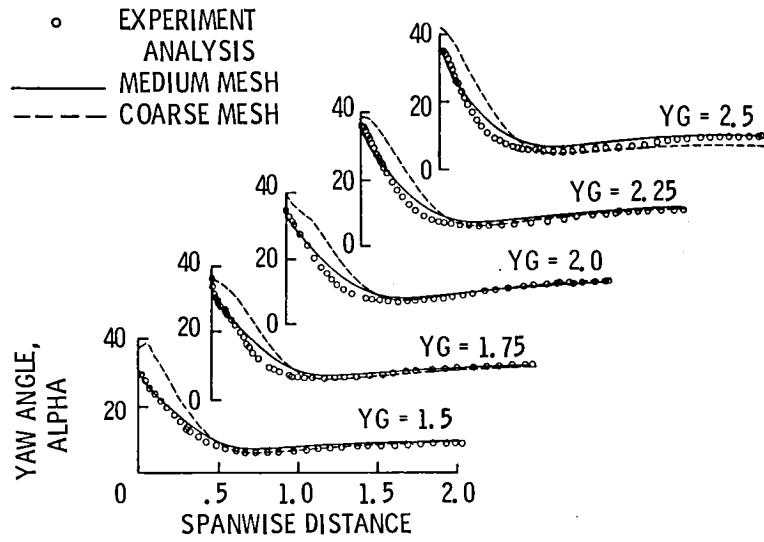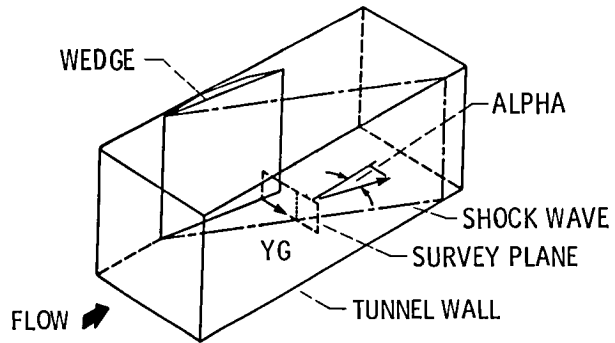
(b) Region of shock wave.

Figure 6. – Continued.

WEDGE

ALPHA

SHOCK
WAVE

YG

SURVEY PLANE

TUNNEL WALL

FLOW

o EXPERIMENT
ANALYSIS
—————— MEDIUM MESH
— — — COARSE MESH
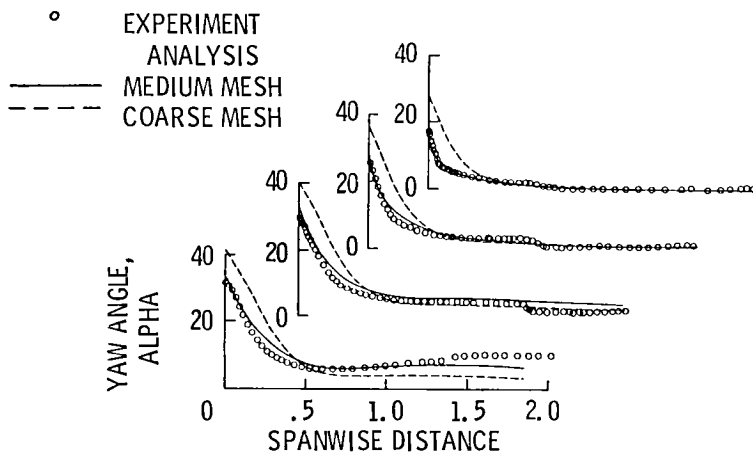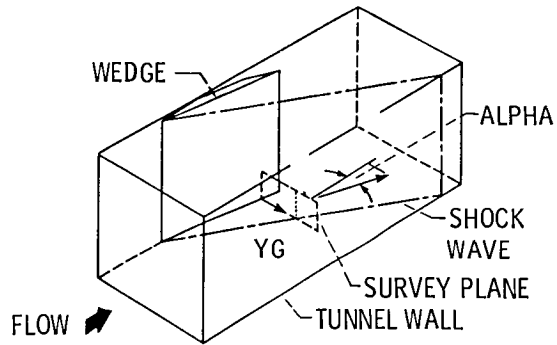
(c) Outer region.

Figure 6. – Concluded.

FLOW

SHOCK WAVE

WEDGE SURFACE

TUNNEL WALL
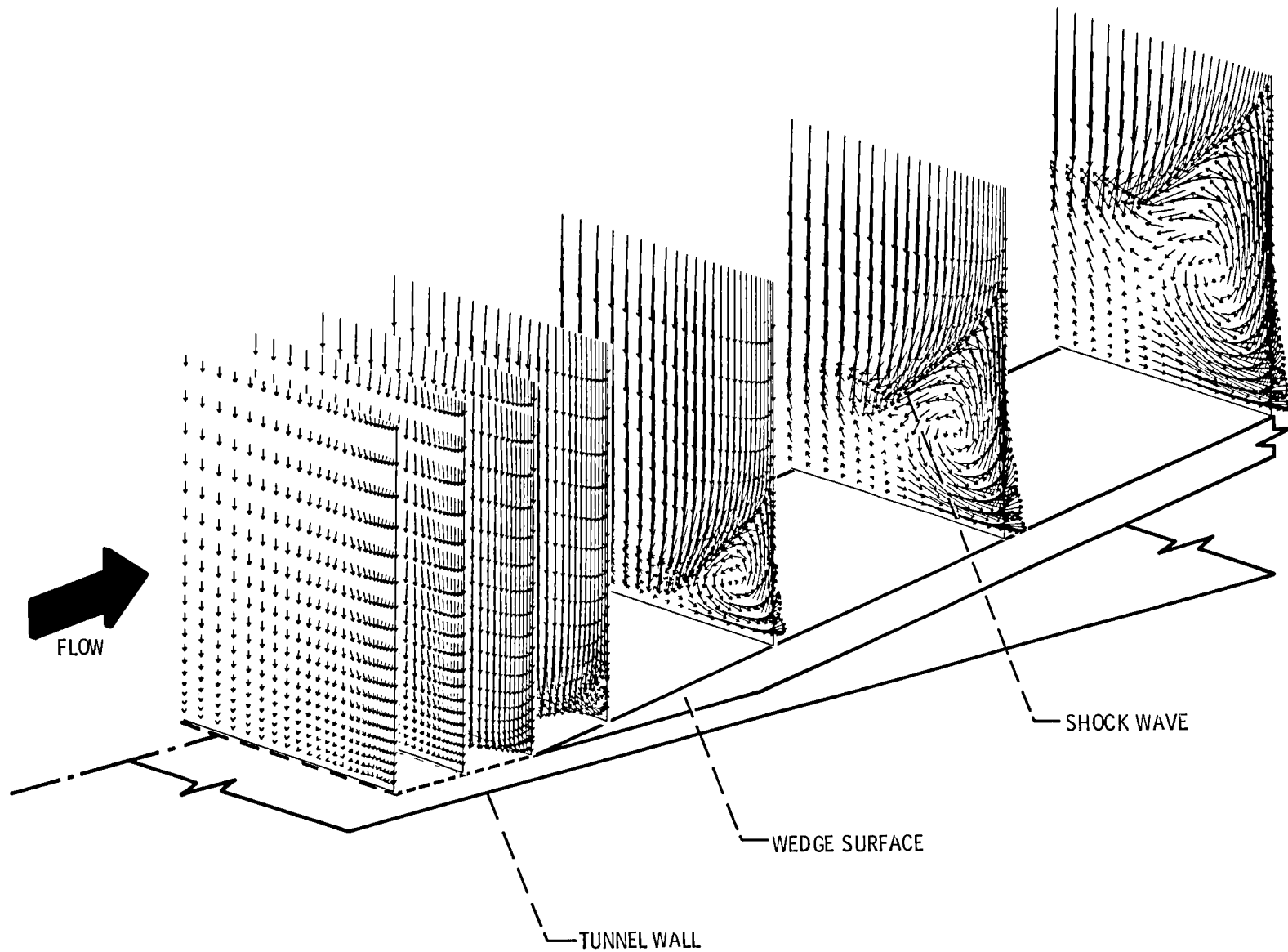
Figure 7. – Three dimensional sidewall shockwave turbulent boundary layer interaction, secondary velocity vectors.
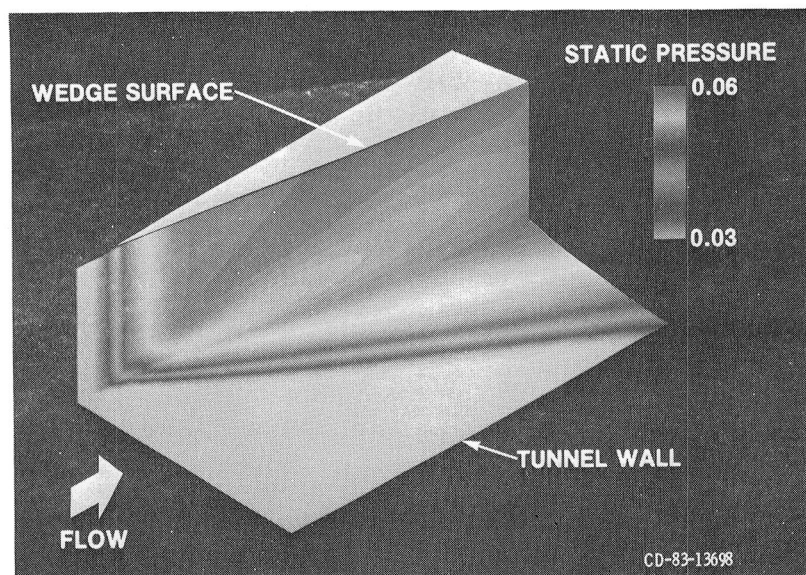
Figure 8. – Three dimensional sidewall shock wave turbulent boundary layer interaction, surface static pressure patterns.
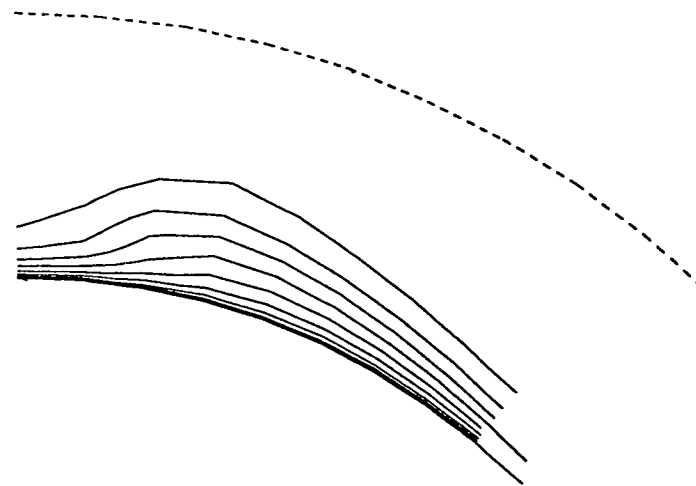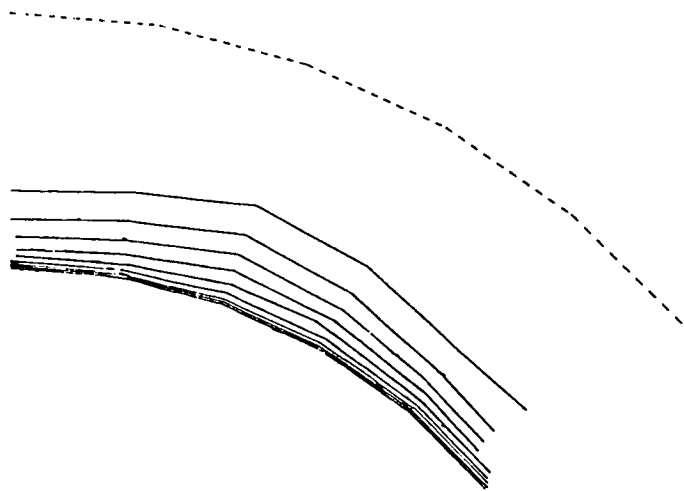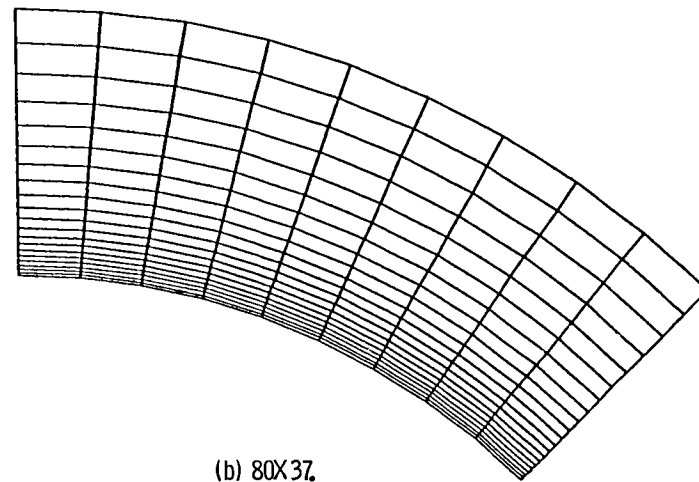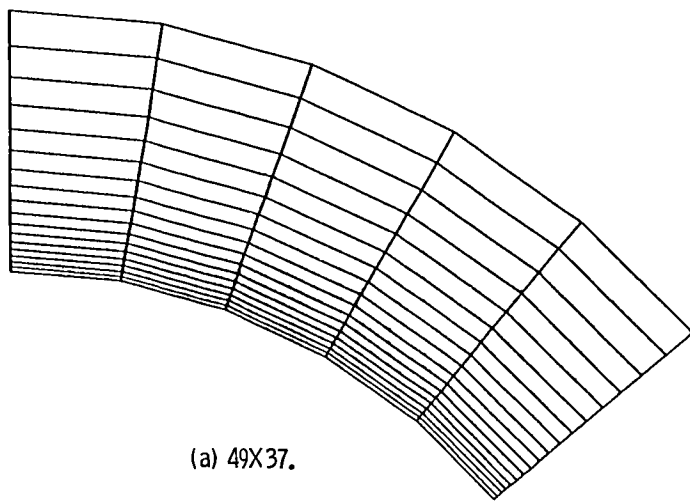
(a) 49X37.

(b) 80X37.

Figure 9. – Three dimensional cone at angle of attack, $M_\infty = 4.25$, $\theta = 12.5^0$, $\alpha = 15.6^0$ mesh resolution study.
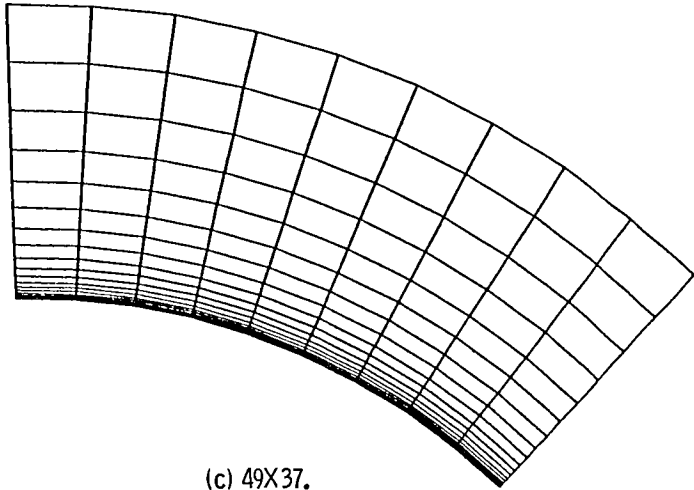
(c) 49X37.
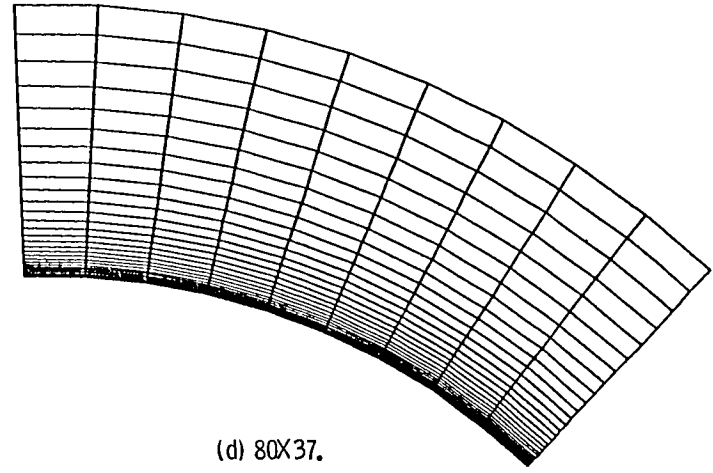
(d) 80X37.

Figure 9. - Continued.

(e) 80X50.

LEEWARD

RECIRCULATION
VORTEX

SHOCK WAVE
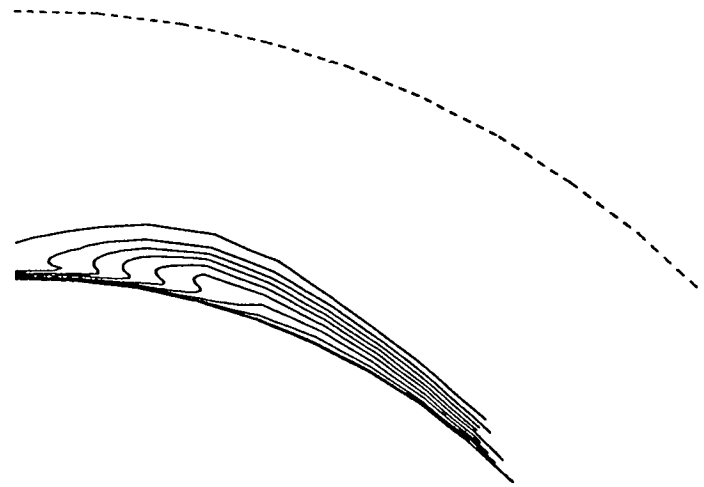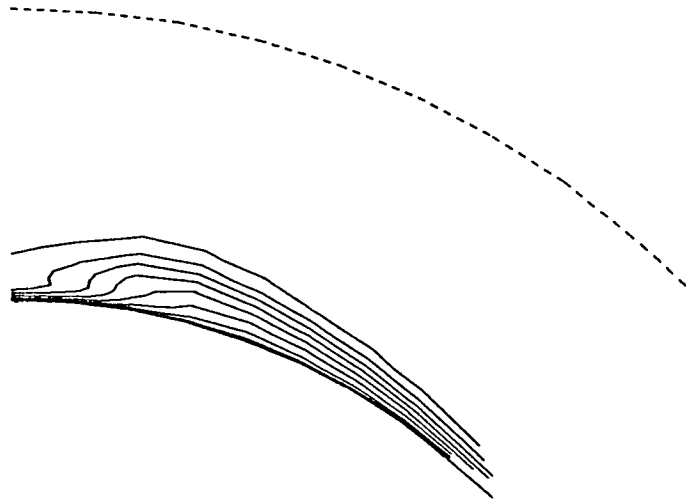
WINDWARD
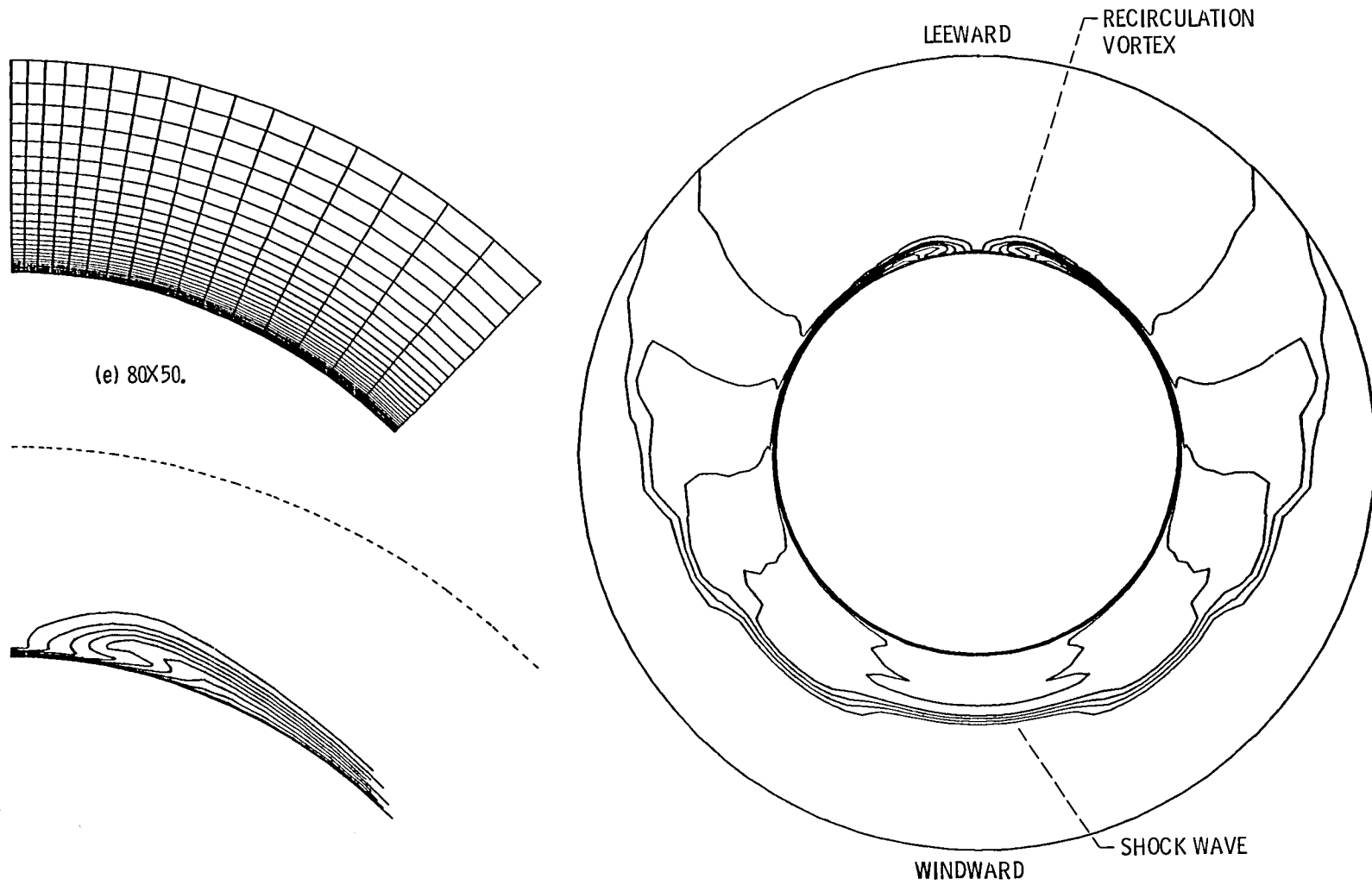
Figure 9. - Concluded.

CONE SURFACE
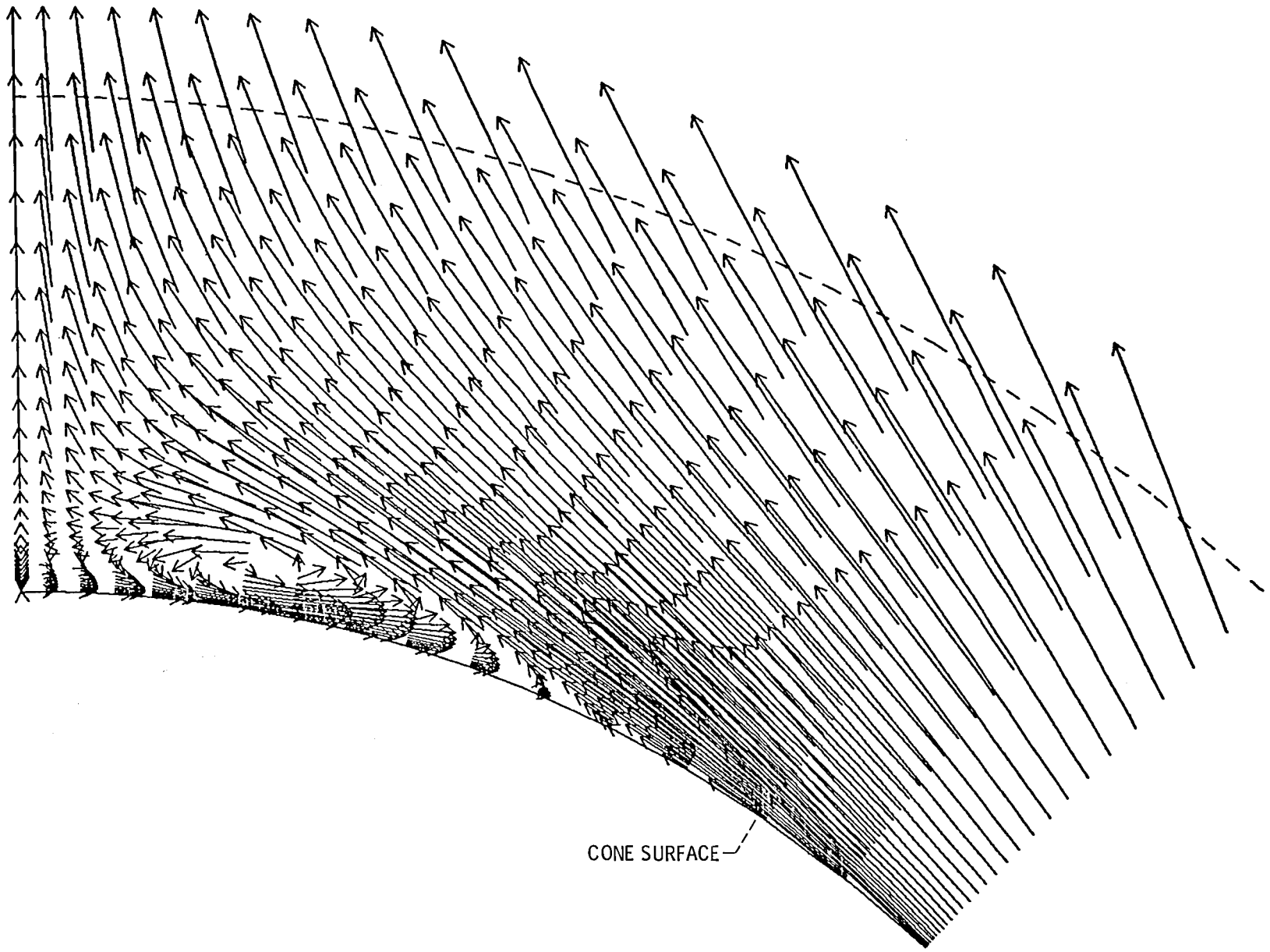
Figure 10. - Three dimensional cone at angle of attack, $M_\infty = 4.25$, $\theta = 12.5^0$, $\alpha = 15.6^0$, structure of recirculation vortex.

PHENOMENON	TYPE OF DATA	STATUS
● 2-D SHOCK/LAM-BL	DETAIL BL SURVEYS	COMPLETED
● 2-D SHOCK/BL/BLEED	DETAIL BL SURVEYS LOCAL BLEED RATES	COMPLETED
● 3-D GLANCING SHOCK/BL	DETAIL BL SURVEYS	START LATE 82
● 3-D GLANCING SHOCK/BL	DETAIL BL SURVEYS LOCAL BLEED RATES	START LATE 84
● 3-D SHOCK/CORNER BL	DETAIL FLOW SURVEYS	START MID 83
● 2-D BL-BLEED TECH.	DETAIL BL SURVEYS LOCAL BLEED RATES TURBULENT BL PROP	START MID 84
● 3-D NORMAL SHOCK/BL	L.D.V. SURVEYS	START LATE 83

Figure 11. – PEPSIS benchmark verification, Lewis 1X1 foot supersonic wind tunnel experiments.
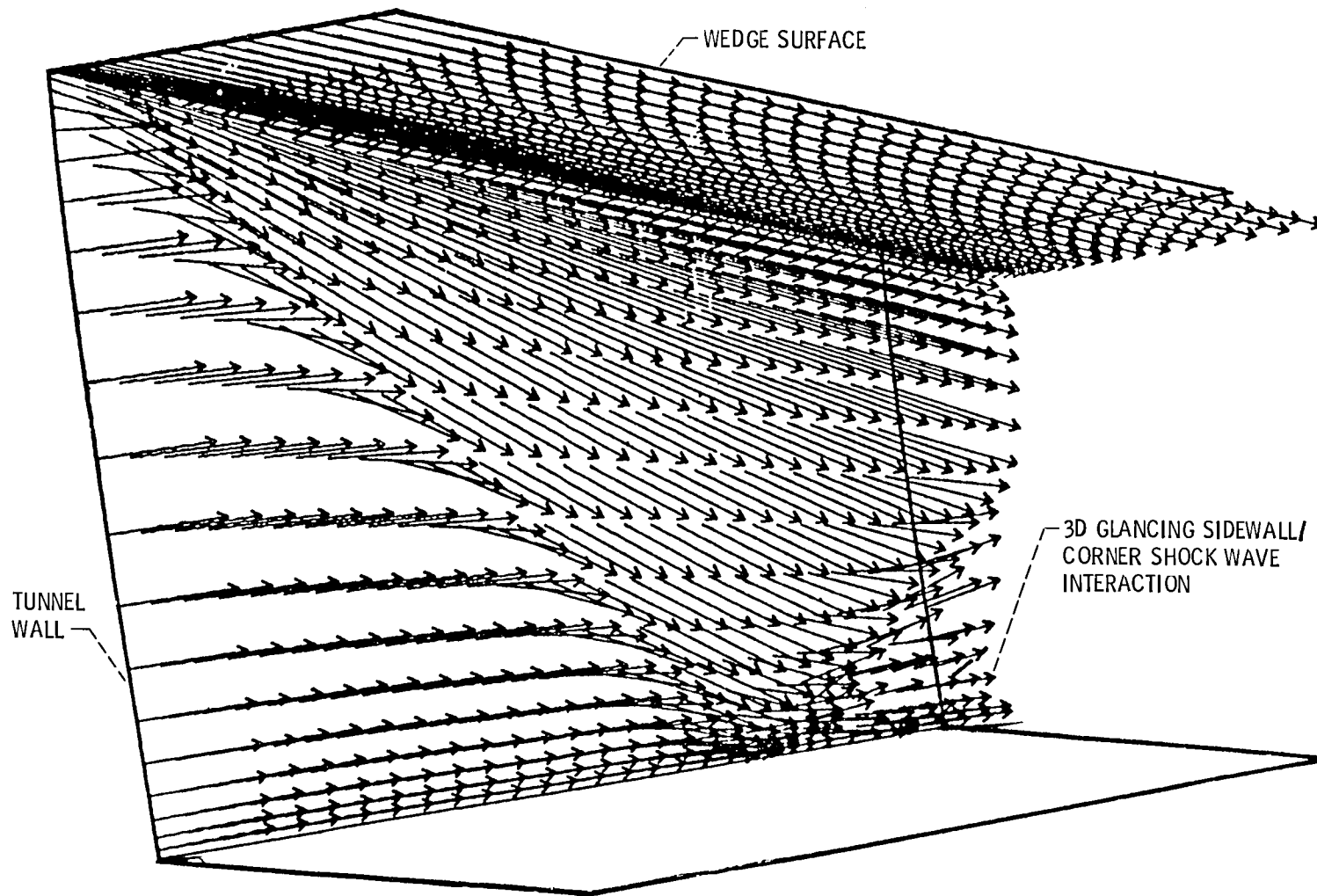
Figure 12. - Three dimensional glancing sidewall/corner shock wave interaction, analytical surface oil film patterns.
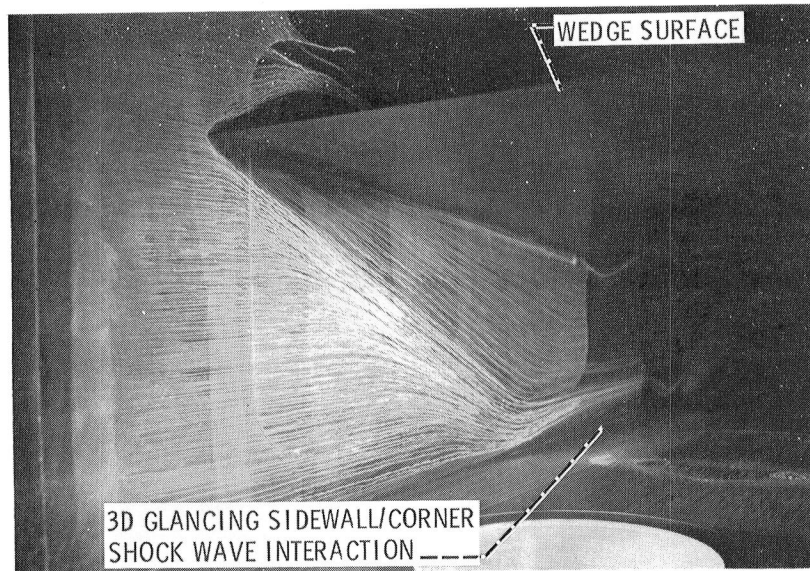
Figure 13. - Three dimensional glancing sidewall/corner interaction, experimental surface oil film patterns.

PHENOMENON	SOURCE	TYPE OF DATA
• HYPERSONIC CORNER	CRESCI	DETAIL BL SURVEYS
• INTERSECTING WEDGE	WEST AND KORKEGI	DETAIL BL SURVEYS
• CROSSED SIDEWALL SHOCK/BL INTERACTION	PROPOSED	DETAIL BL SURVEYS
• SKEWED WEDGE	SETTLES AND BOGDONOFF	DETAIL BL SURVEYS

Figure 14. - PEPSIS benchmark verification for advanced aircraft inlet concepts.

BOUNDARY
LAYER

BOUNDARY
LAYER SHOCK

CORNER SHOCK

SLIP SURFACE

EMBEDDED
SHOCK
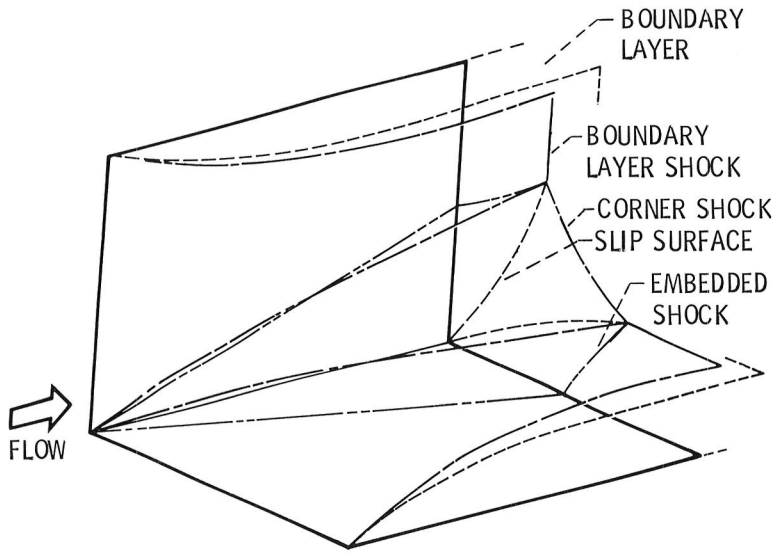
FLOW

Figure 15. – Hypersonic corner interaction, shock wave structure.

BOUNDARY LAYER SHOCK

CORNER SHOCK

EMBEDDED SHOCK

SLIP SURFACE

MACH NO.

11.0

0.0
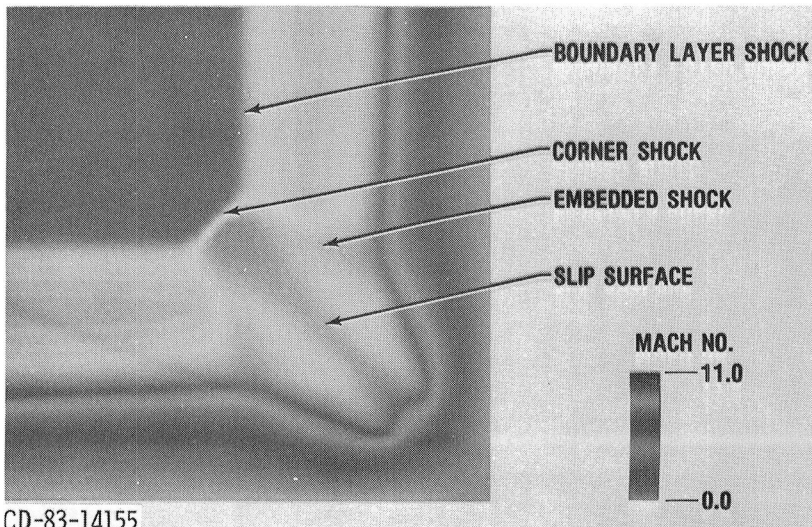
CD-83-14155

Figure 16. – Hypersonic corner interaction, Mach number signature.
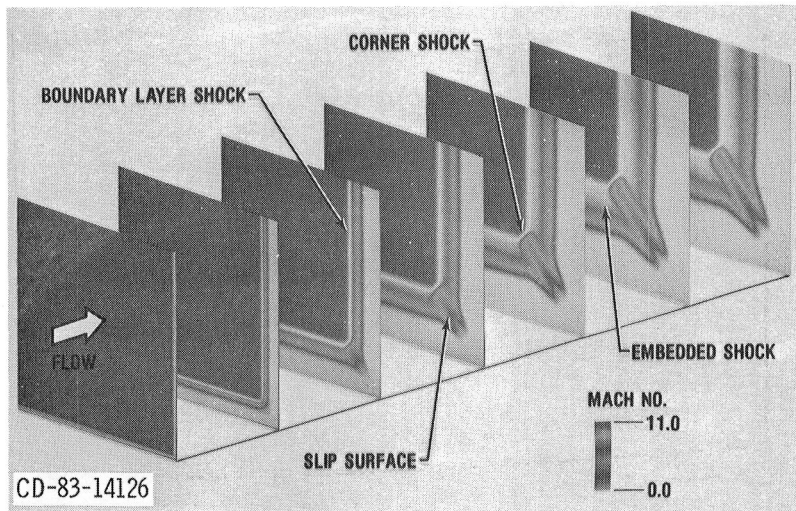
Figure 17. - Hypersonic corner interaction, flow field total pressure signature.
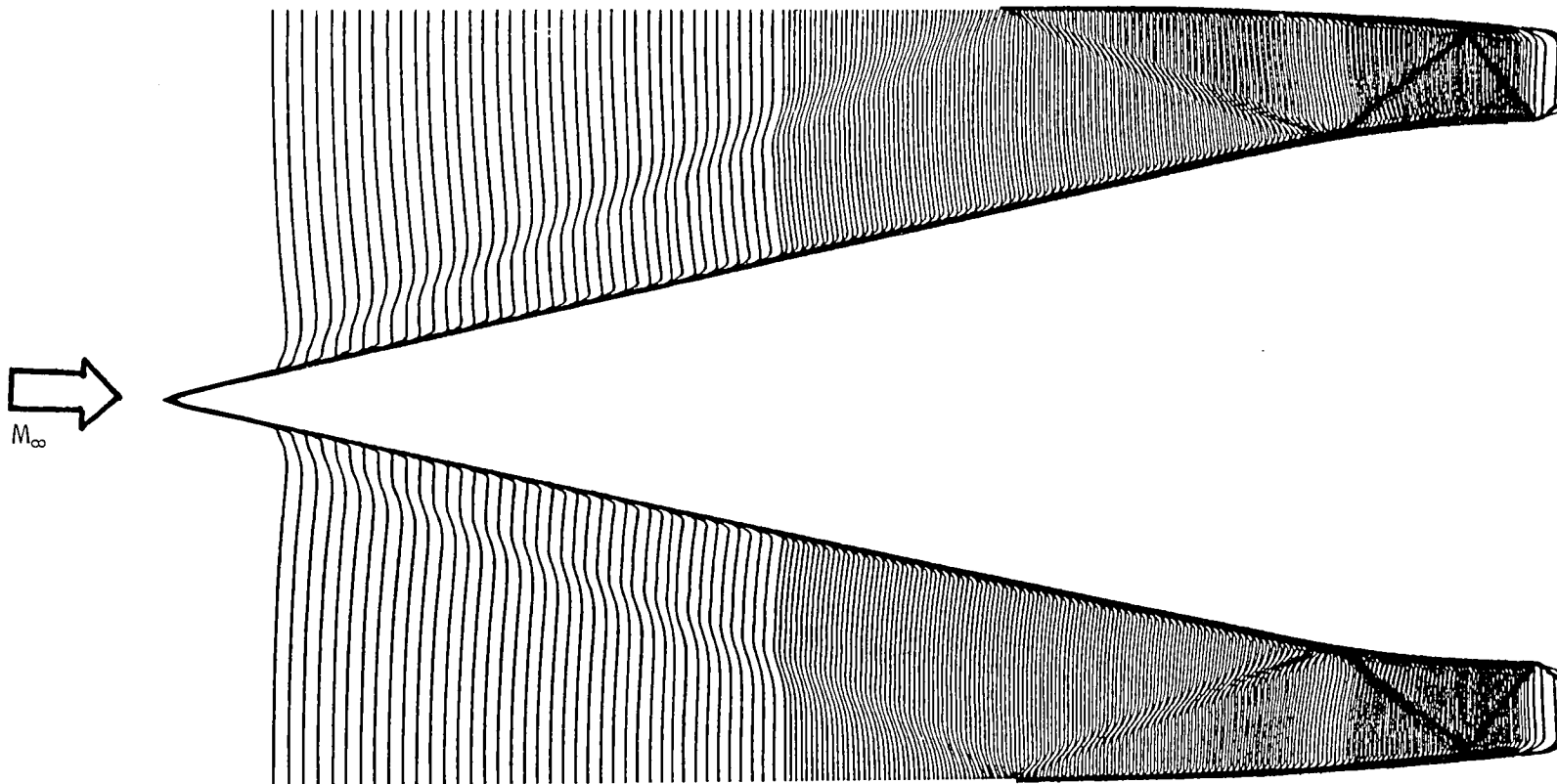
Figure 18. – Lewis 40/60 mixed compression supersonic inlet, Mach number profiles, $M_\infty = 2.5, \alpha = 0.0^0$.
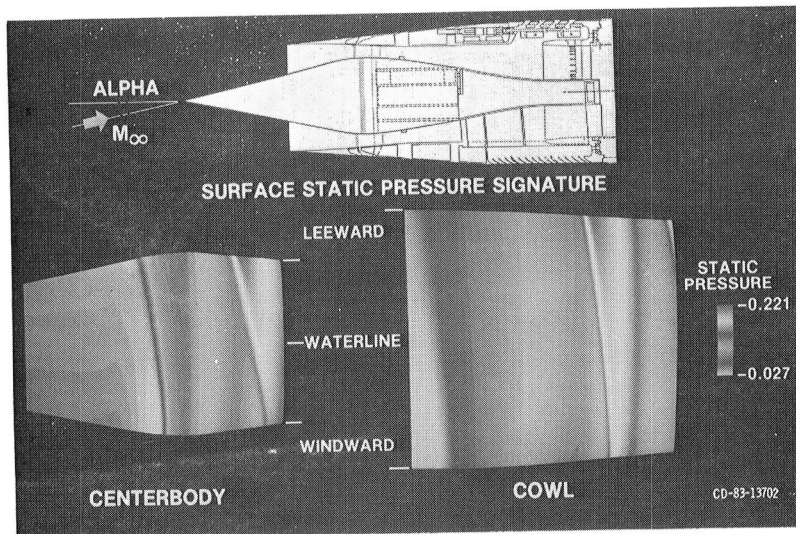
Figure 19. - Lewis 40/60 mixed compression supersonic inlet, surface static pressure, $M_\infty = 3.0$, $\alpha = 2.0^0$.
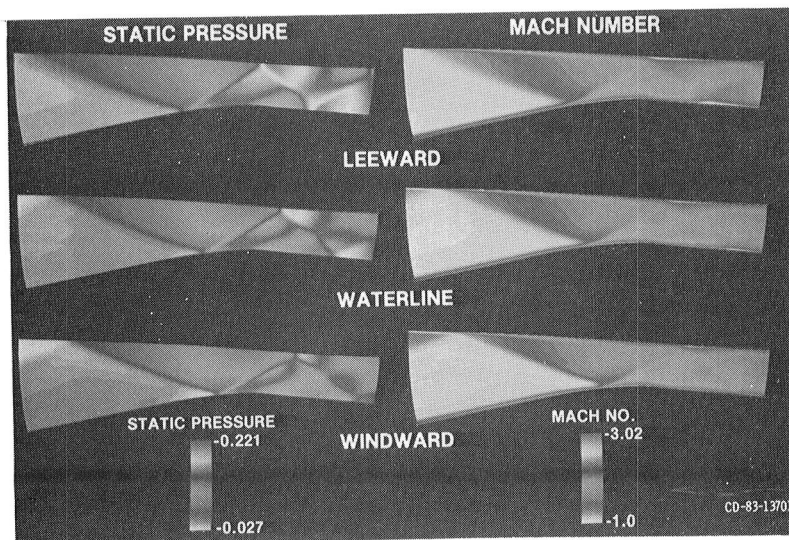
Figure 20. - Lewis 40/60 mixed compression supersonic inlet, flow field static pressure and mach number $M_\infty = 3.0$, $\alpha = 2.0^0$.

PHENOMENON	SOURCE	TYPE OF DATA
● 2D STEADY N-SHOCK BL INTERACTION	MATEER CHANNEL	DETAIL BL SURVEYS
	SAJBEN DIFF	FLOW FIELD SURVEYS STATIC PRESS
● 2D UNSTEADY N-SHOCK BL INTERACTION	SAJBEN DIFF	STATIC PRESS
● 3D STEADY N-SHOCK BL INTERACTION	1X1 LEWIS	3 COMP LDV

Figure 21. - MINT benchmark verification.

STATIC PRESSURE CONTOURS

◊ EXPERIMENT

— ANALYSIS

PRESSURE

DISTANCE
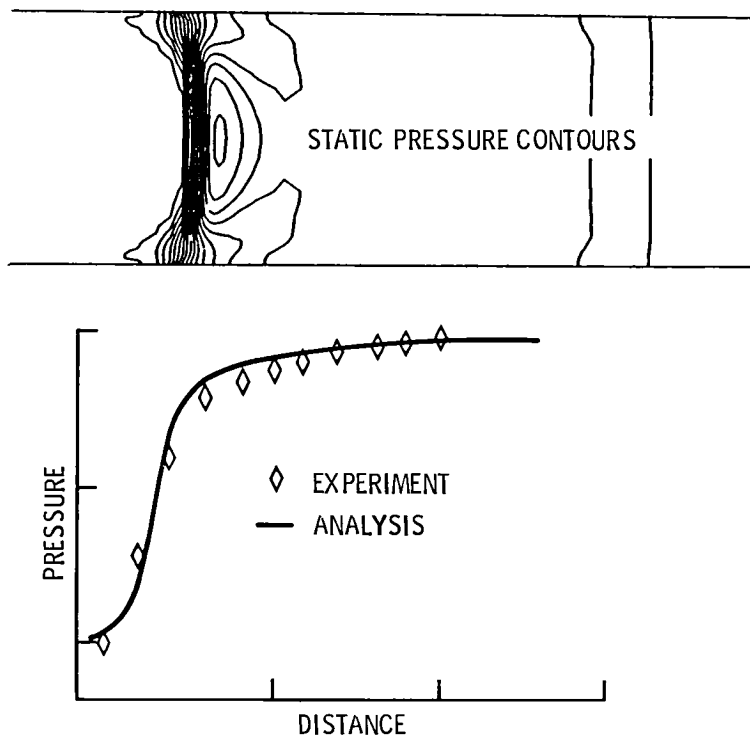
Figure 22. - Constant area normal shock wave interaction, static pressure.
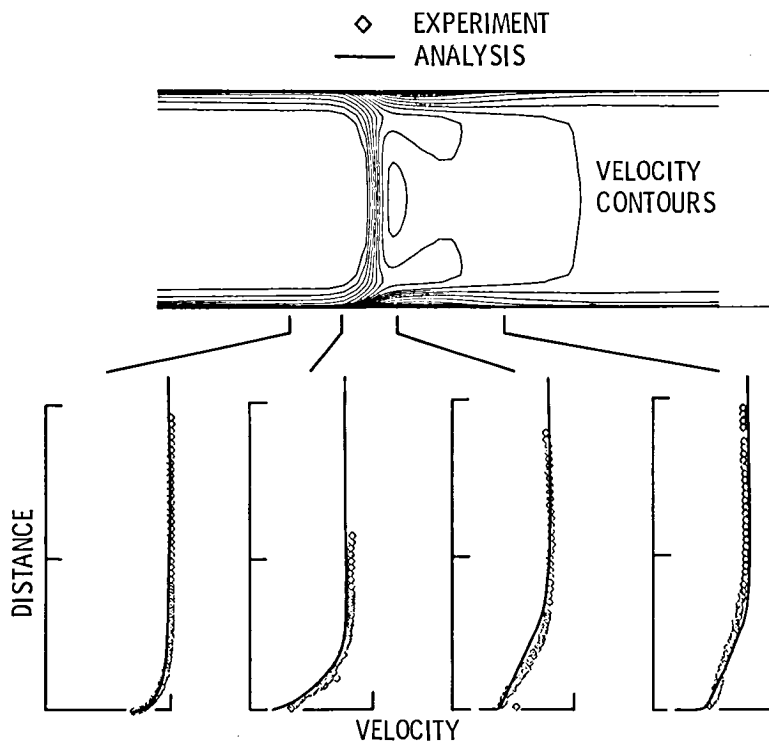
Figure 23. – Constant area normal shock wave interaction velocity profiles.

STATIC PRESSURE CONTOURS

(a) Bottom wall static pressure.

STATIC PRESSURE CONTOURS

EXPERIMENT
ANALYSIS
σ = 0.05
σ = 0.5

DISTANCE

(b) Top wall static pressure.
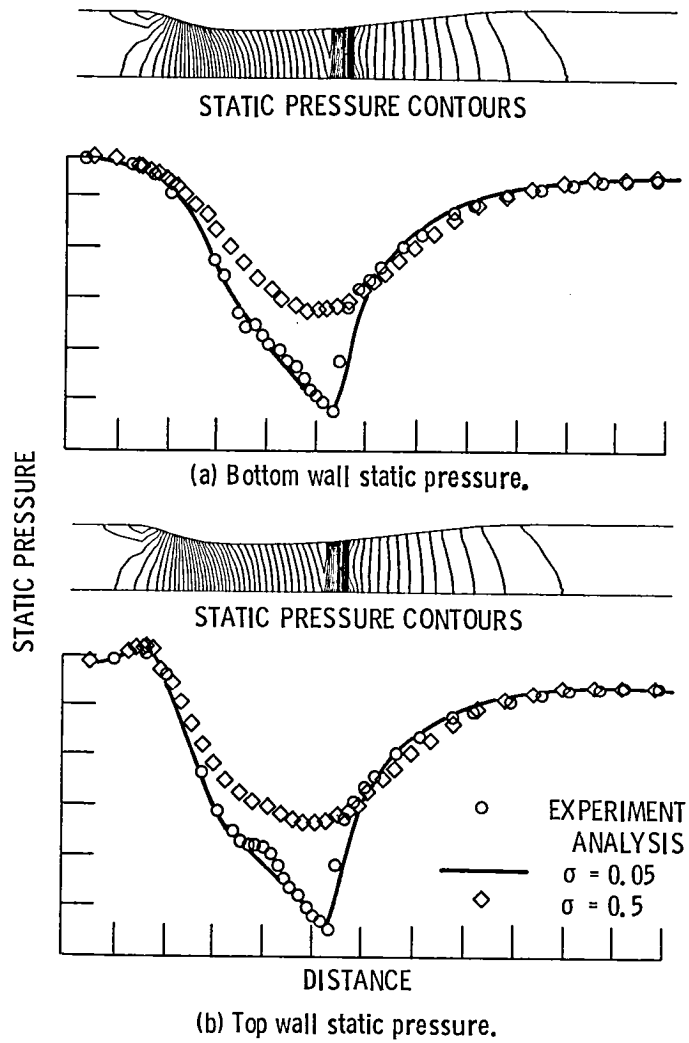
Figure 24. - Variable area normal shock wave interaction.

PHENOMENON	SOURCE	TYPE OF DATA
● SEC. FLOW GEN.	WHITELAW 90	3-COMP. LDV
	AGRAWAL 180	2-COMP. LDV
	ROWE 180	TOTAL PRESS.
● SEC. FLOW DECAY	WHITELAW 90	3-COMP. LDV
	ROWE 180	TOTAL PRESS.
● REVERSE CURV.	WHITELAW 22.5-22.5	3-COMP. LDV
	TENN. 30-30	3-COMP. PROBE
	BRADSHAW 45-45	TOTAL PRESS.
	ROWE 45-45	TOTAL PRESS.
● X-SECT. TRANS.	WHITELAW TRANS.	3-COMP. LDV
● DIFFUSION	TENN. 30-30	3-COMP. PROBE
	WHITELAW DIFF.	3-COMP. LDV
● COMPRESSIBILITY	TENN. 30-30	3-COMP. PROBE

Figure 25. – PEPSIG benchmark verification.
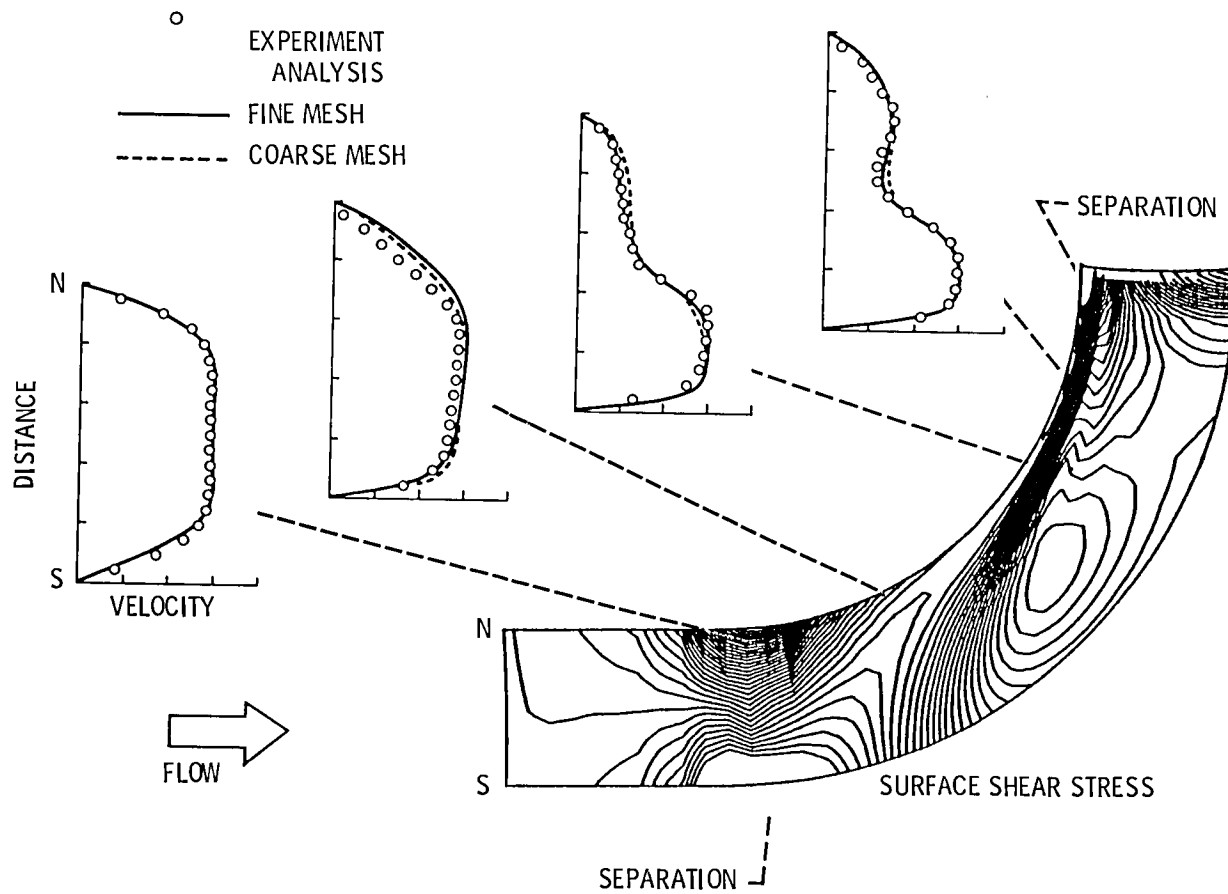
Figure 26. – Circular 90° bend, laminar flow, streamwise velocity.

SEPARATION

N

S

FLOW

SURFACE OIL
FLOW PATTERNS

SEPARATION
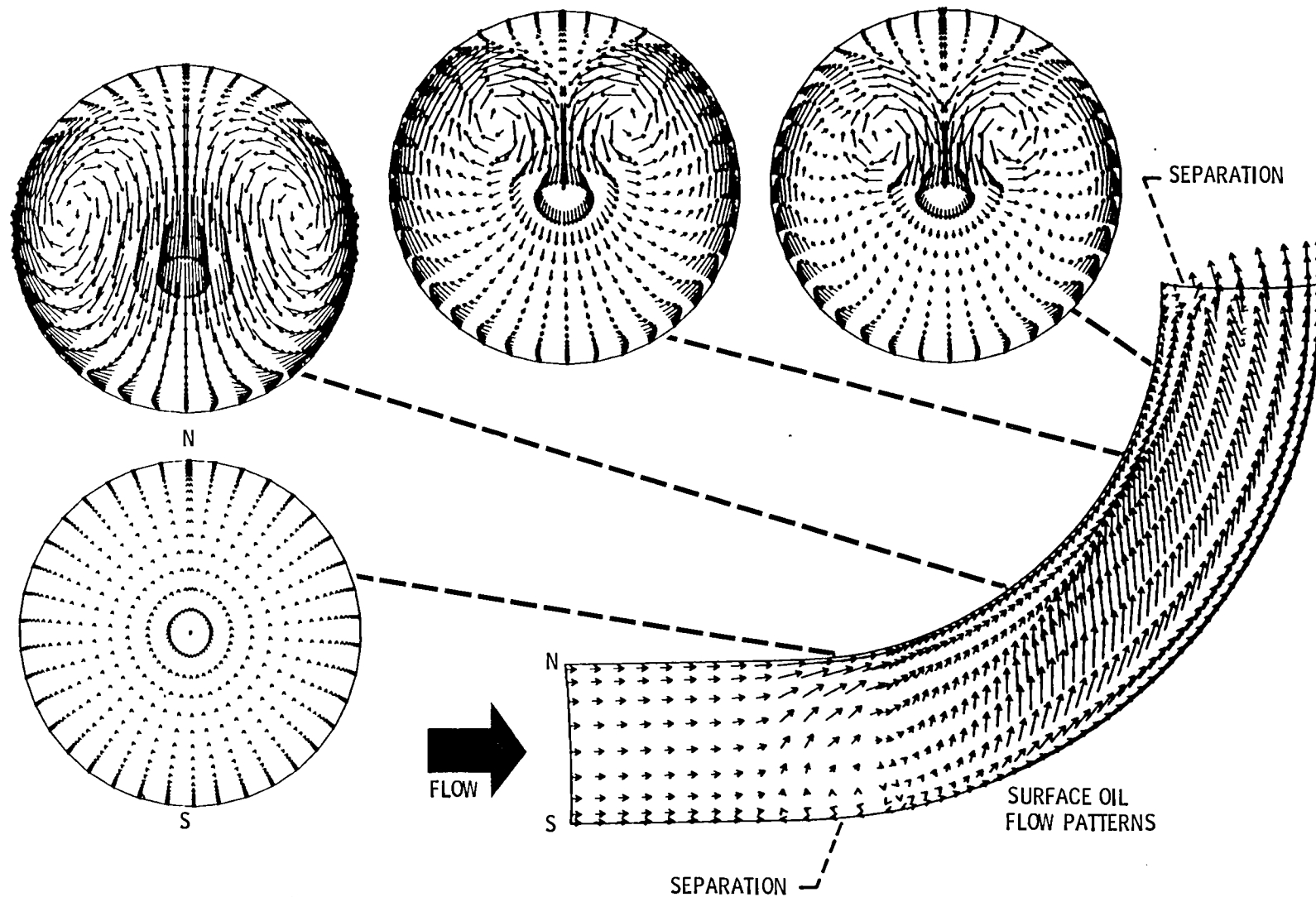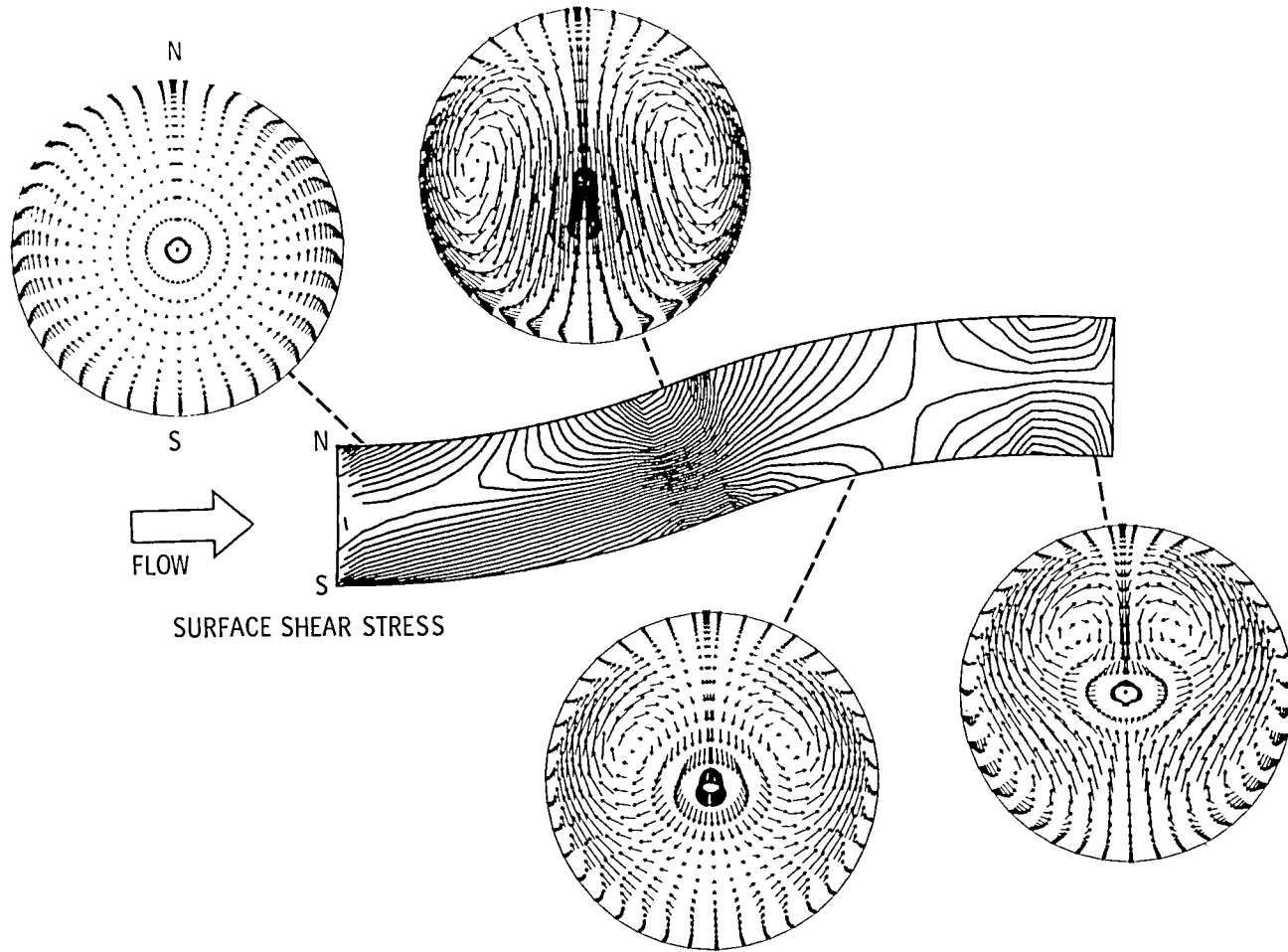
Figure 27. – Circular 90° bend, laminar flow, secondary velocity.
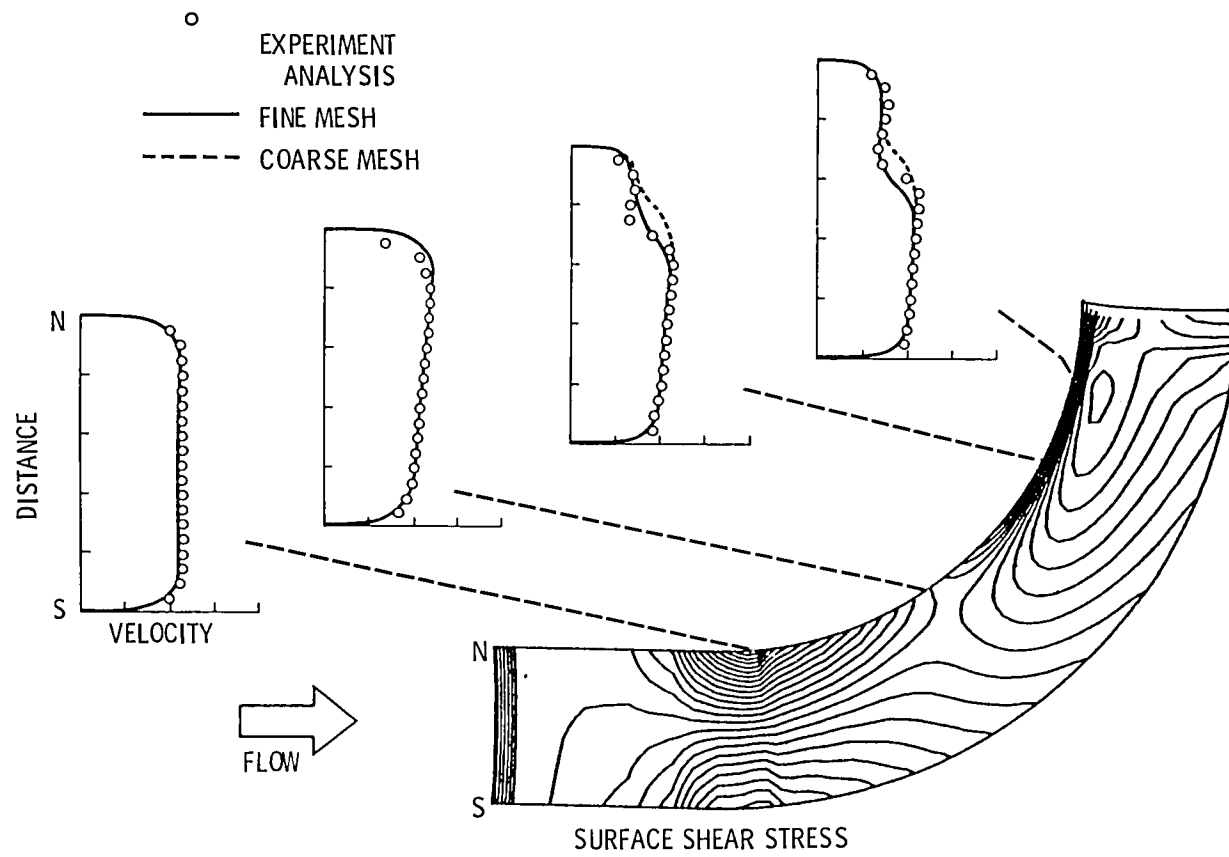
Figure 28. - Circular 90° bend, turbulent flow, streamwise velocity.

N

S

FLOW

N

S

SURFACE OIL FLOW PATTERNS
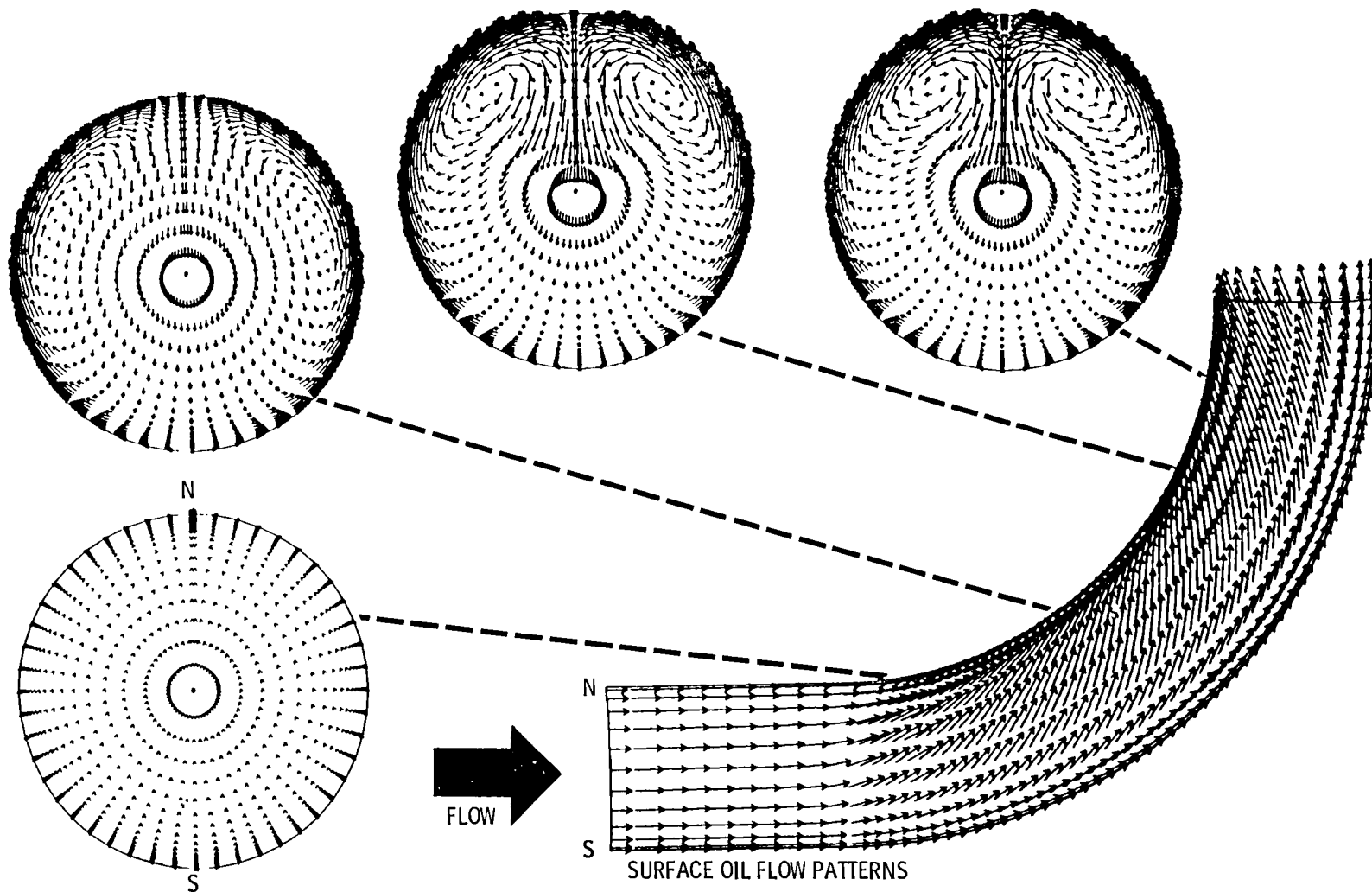
Figure 29. – Circular 90° bend, turbulent flow, secondary velocity.
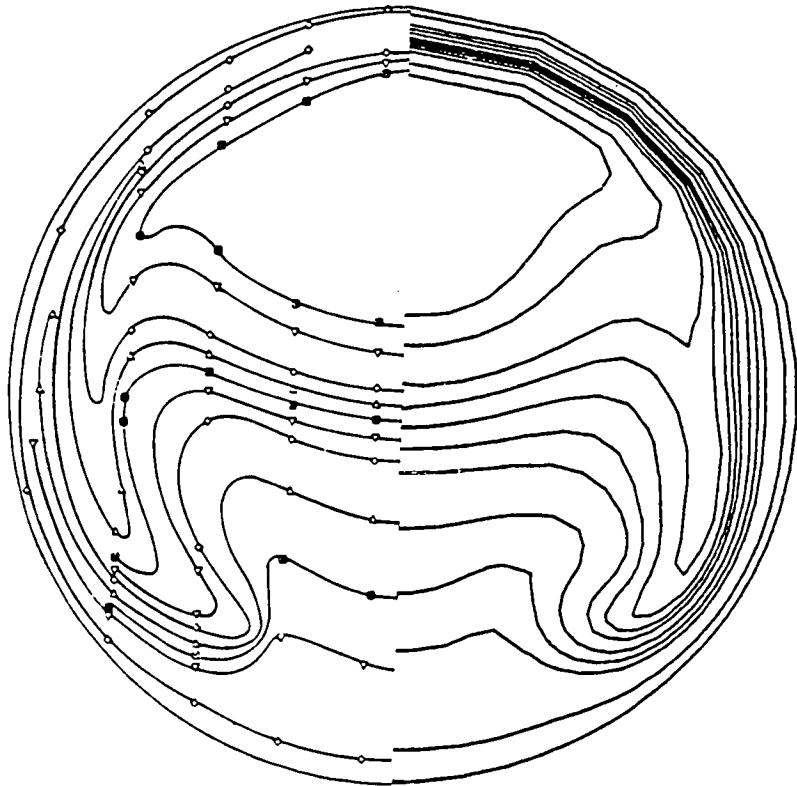
EXPERIMENT   ANALYSIS
STREAMWISE VELOCITY
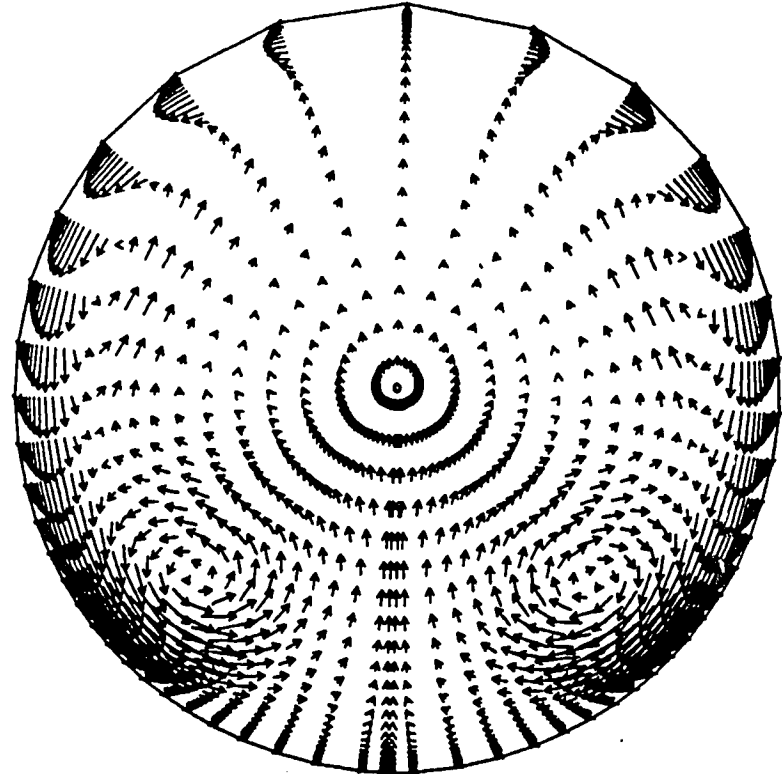
SECONDARY VELOCITY

Figure 30. - Circular 180° bend, laminar flow.
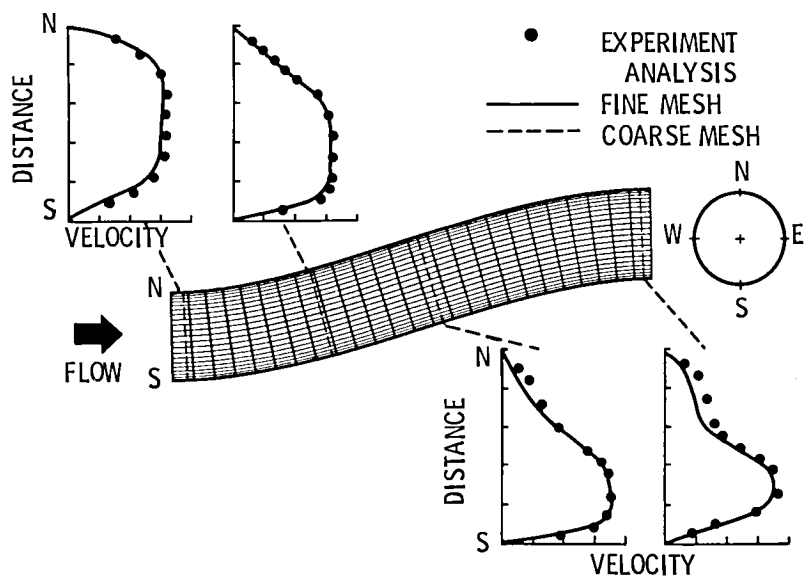
Figure 31. – Circular 22.5-22.5° S-bend, laminar flow, streamwise velocity.

N

S

N

S

FLOW

SURFACE SHEAR STRESS

Figure 32. - Circular 22.5-22.5° S-bend, laminar flow, secondary velocity.
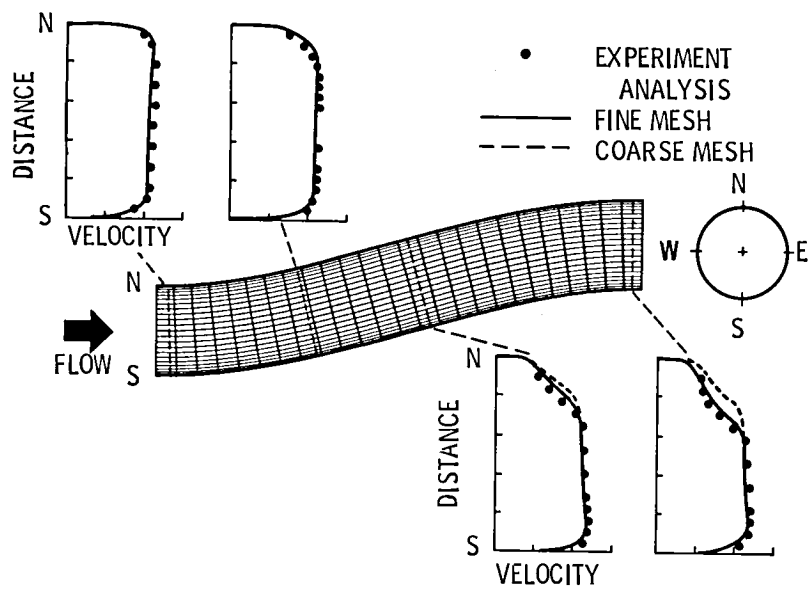
Figure 33. – Circular 22.5-22.5° S-bend turbulent flow, streamwise velocity.
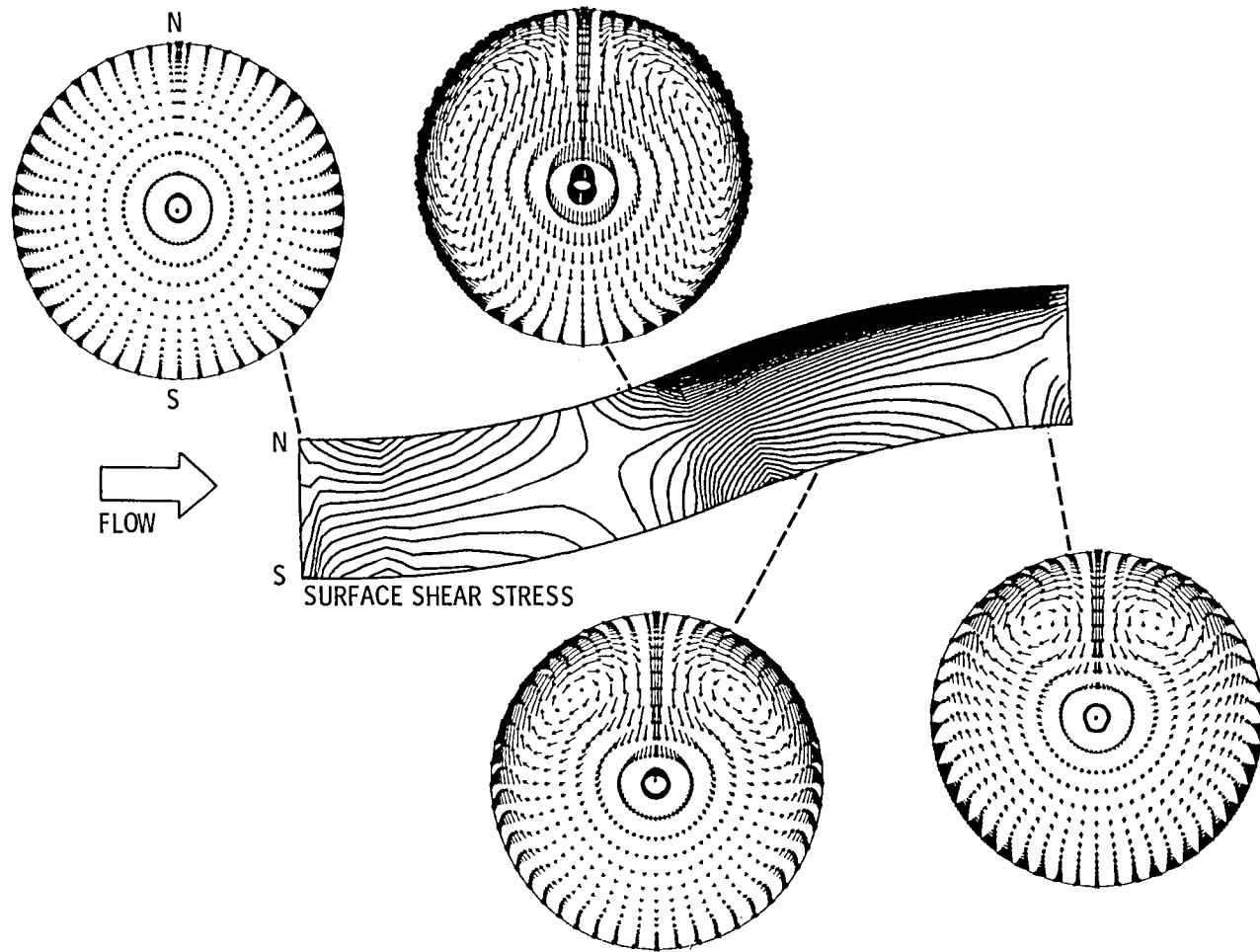
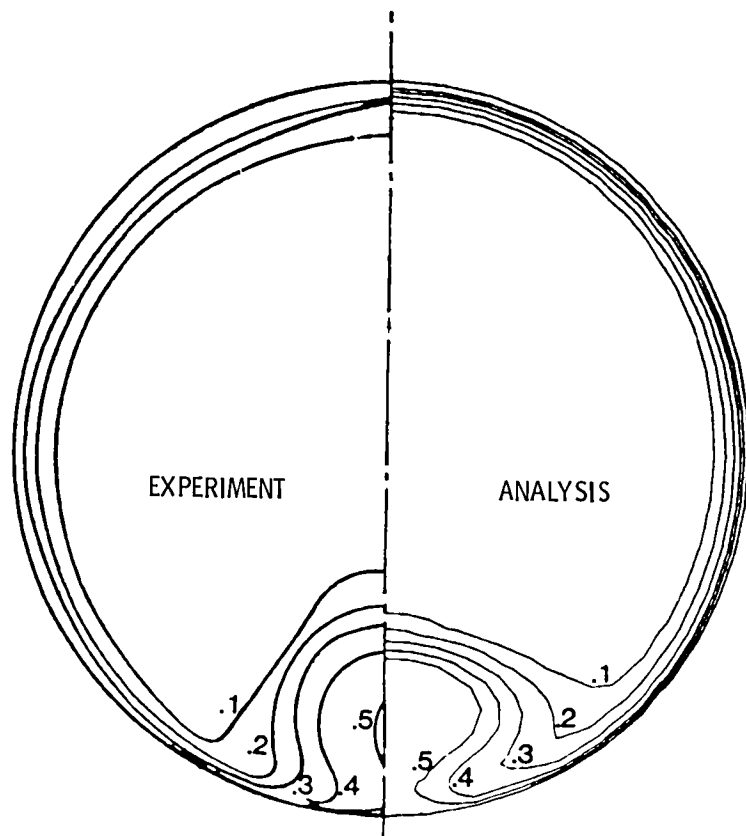Figure 34. - Circular 22.5° S-bend, turbulent flow, secondary velocity.
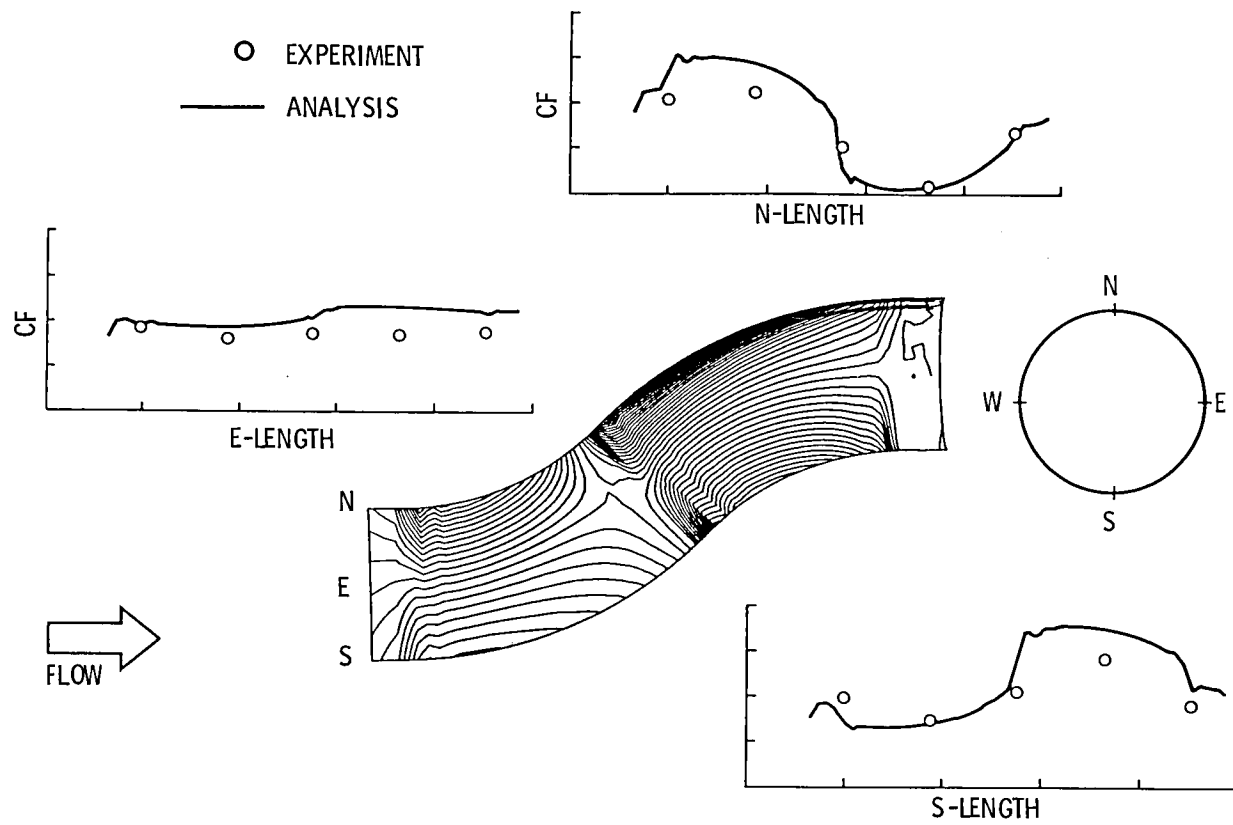
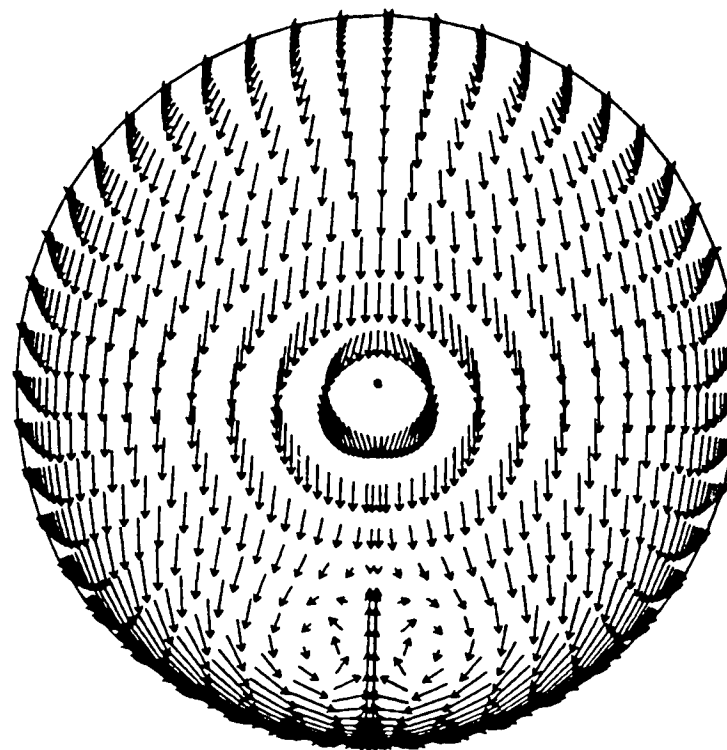Figure 35. - Circular 45-45° S-bend, turbulent flow, wall shear stress.

EXPERIMENT   ANALYSIS

TOTAL PRESSURE LOSS   SECONDARY VELOCITY

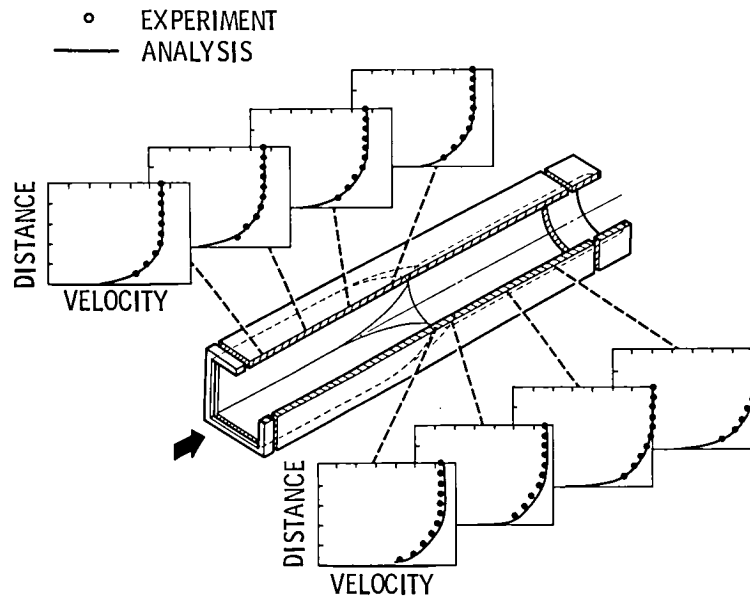Figure 36. - Circular 45-45° S-bend, turbulent flow, compressor face station.

o   EXPERIMENT

—— ANALYSIS

DISTANCE

VELOCITY

DISTANCE

VELOCITY

Figure 37. - Square-to-round transition duct, turbulent flow,
streamwise velocity.

COMPRESSOR FACE⌐

⌐INLET FACE

FLOW

STATIC PRESSURE

FLOW

ANALYTICAL OIL FILM PATTERNS
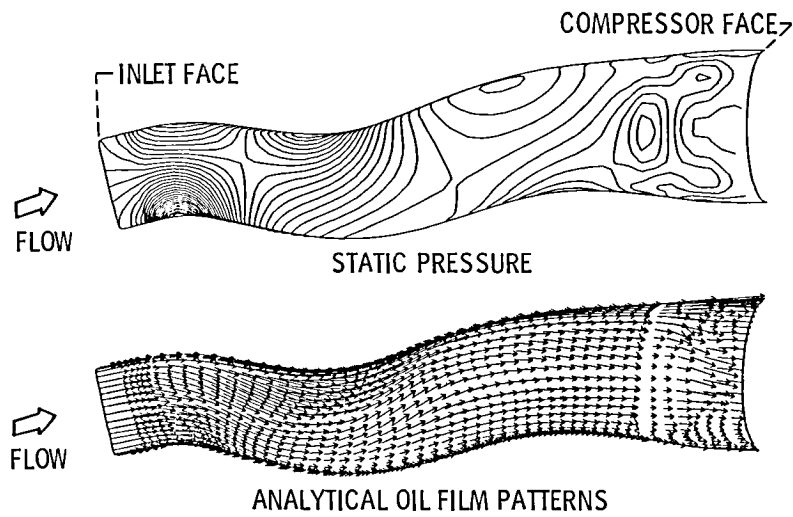
Figure 38. - Rockwell BIB inlet duct surface conditions.

FLOW ⇨

INLET FACE

COMPRESSOR FACE

PT/PTO

0.99

.97

.95

.93

TOTAL PRESSURE

SECONDARY VELOCITY
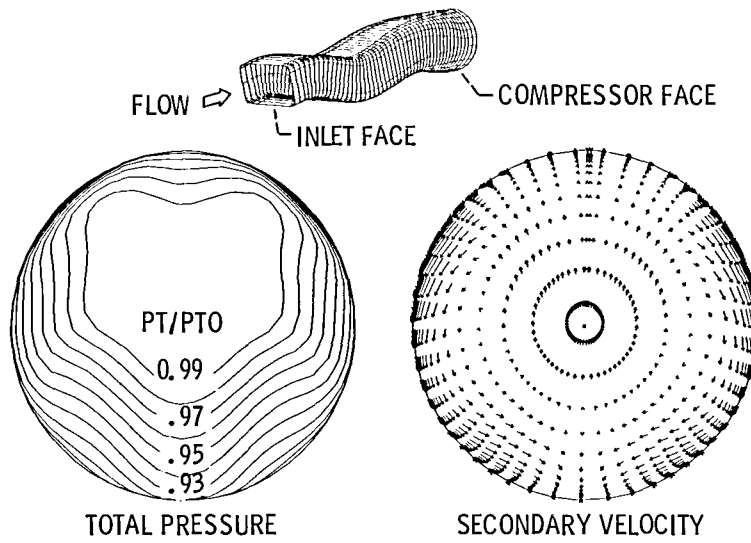
Figure 39. - Rockwell BIB inlet duct, compressor face station.

1. Report No. NASA TM-83558 AIAA-84-0192	2. Government Accession No.	3. Recipient's Catalog No.
4. Title and Subtitle Three-Dimensional Viscous Design Methodology for Advanced Technology Aircraft Supersonic Inlet Systems		5. Report Date
		6. Performing Organization Code 505-34-01B
7. Author(s) Bernhard H. Anderson		8. Performing Organization Report No. E-1936
		10. Work Unit No.
9. Performing Organization Name and Address National Aeronautics and Space Administration Lewis Research Center Cleveland, Ohio 44135		11. Contract or Grant No.
		13. Type of Report and Period Covered Technical Memorandum
12. Sponsoring Agency Name and Address National Aeronautics and Space Administration Washington, D.C. 20546		14. Sponsoring Agency Code

15. Supplementary Notes

Prepared for the Twenty-second Aerospace Sciences Meeting sponsored by the American Institute of Aeronautics and Astronautics, Reno, Nevada, January 9-12, 1984.

16. Abstract

The present report discusses a broad program to develop advanced, reliable, and user oriented three-dimensional viscous design techniques for supersonic inlet systems, and encourage their transfer into the general user community. This program is fourfold in nature, namely (1) develop effective methods of computing three-dimensional flows within a zonal modeling methodology, (2) ensure reasonable agreement between said analysis and selective sets of benchmark validation data, (3) develop "user" orientation into said analysis, and (4) explore and develop advanced numerical methodology.

17. Key Words (Suggested by Author(s)) Propulsion Aerodynamics Computations	18. Distribution Statement Unclassified - unlimited STAR Category 07		
19. Security Classif. (of this report) Unclassified	20. Security Classif. (of this page) Unclassified	21. No. of pages	22. Price*

National Aeronautics and
Space Administration

Washington, D.C.
20546

SPECIAL FOURTH CLASS MAIL
BOOK

NASA